Journal of Hydrology 523 (2015) 211–230

Contents lists available at ScienceDirect

Journal of Hydrology

journal homepage: www.elsevier.com/locate/jhydrol

Precipitation extremes over La Plata Basin – Review and new results from observations and climate simulations

I.F.A. Cavalcanti [a,*], A.F. Carril [e,h], O.C. Penalba [b,h], A.M. Grimm [c], C.G. Menéndez [b,e,h], E. Sanchez [d], A. Cherchi [f], A. Sörensson [e,h], F. Robledo [b,e,h], J. Rivera [b], V. Pántano [b], L.M. Bettolli [b], P. Zaninelli [e,h], L. Zamboni [g], R.G. Tedeschi [a], M. Dominguez [d], R. Ruscica [e,h], R. Flach [c]

[a] Centro de Previsão de Tempo e Estudos Climáticos, Instituto Nacional de Pesquisas Espaciais (CPTEC/INPE), Brazil
[b] Departamento de Ciencias de la Atmósfera y los Océanos, FCEN, UBA, Buenos Aires, Argentina
[c] Universidade Federal do Paraná, Curitiba, Brazil
[d] University of Castilla-La Mancha, Spain
[e] Centro de Investigaciones del Mar y la Atmósfera (CIMA/CONICET-UBA), Argentina
[f] Centro Euro-Mediterraneo sui Cambiamenti Climatici and Istituto Nazionale di Geofisica e Vulcanologia, Bologna, Italy
[g] Argonne National Laboratory, MCS Division, USA
[h] UMI-IFAECI/CNRS-CONICET-UBA, Argentina

ARTICLE INFO

Article history:
Received 22 January 2014
Received in revised form 15 December 2014
Accepted 10 January 2015
Available online 28 January 2015
This manuscript was handled by Konstantine P. Georgakakos, Editor-in-Chief, with the assistance of Ercan Kahya, Associate Editor

Keywords:
Precipitation extremes
La Plata Basin
South America
Large-scale features
Soil moisture
Model simulations

SUMMARY

Monthly and daily precipitation extremes over La Plata Basin (LPB) are analyzed in the framework of the CLARIS-LPB Project. A review of the studies developed during the project and results of additional research are presented and discussed. Specific aspects of analysis are focused on large-scale versus local processes impacts on the intensity and frequency of precipitation extremes over LPB, and on the assessment of specific wet and dry spell indices and their changed characteristics in future climate scenarios. The analysis is shown for both available observations of precipitation in the region and ad-hoc global and regional models experiments. The Pacific, Indian and Atlantic Oceans can all impact precipitation intensity and frequency over LPB. In particular, considering the Pacific sector, different types of ENSO events (i.e. canonical vs Modoki or East vs Central) have different influences. Moreover, model projections indicate an increase in the frequency of precipitation extremes over LPB during El Niño and La Niñā events in future climate. Local forcings can also be important for precipitation extremes. Here, the feedbacks between soil moisture and extreme precipitation in LPB are discussed based on hydric conditions in the region and model sensitivity experiments. Concerning droughts, it was found that they were more frequent in the western than in the eastern sector of LPB during the period of 1962–2008. On the other hand, observations and model experiments agree in that the monthly wet extremes were more frequent than the dry extremes in the northern and southern LPB sectors during the period 1979–2001, with higher frequency in the south.

1. Introduction

Extreme precipitation events in the La Plata Basin (LPB) region cause intense damage to agriculture, cattle raising, and water resources and have also an impact on urban areas due to flooding and landslides. The basin is the second largest in South America, encompassing four countries: Argentina, Brazil, Paraguay and Uruguay (Fig. 1). It has the largest population density of the continent and the largest hydroelectric power plant (Itaipu), which provides energy to several regions. La Plata Basin is also the most productive region in agriculture, with soybean, maize, cotton, sugar/alcohol, rice, wheat, coffee, and orange products. Therefore precipitation extremes occurring in LPB can largely affect the social and economic sectors of the continent. Floods can occur as a result of heavy and persistent precipitation over the region and also from overflow of the main basin rivers (Parana, Paraguay, and Uruguay rivers). Periods of extremely dry conditions affect as well the agriculture, and undermine the water resources needed for hydroelectricity power.

The region undergoes interdecadal, interannual, and intraseasonal variability (Robertson and Mechoso, 1998; Grimm et al., 2000; Nogués-Paegle and Mo, 1997). Moreover, it is influenced

* Corresponding author at: CPTEC/INPE, Rodovia Presidente Dutra, Km 40, Cachoeira Paulista, São Paulo, Brazil. Tel.: +55 12 32086027.
E-mail address: iracema@cptec.inpe.br (I.F.A. Cavalcanti).

http://dx.doi.org/10.1016/j.jhydrol.2015.01.028
0022-1694/

by teleconnections such as the Pacific South America (PSA) pattern (Cunningham and Cavalcanti, 2006; Zamboni et al., 2012; Cherchi et al., 2014) and blocking episodes (Mendes et al., 2008). The LPB region is also influenced by sea surface temperature (SST) forcing in both the Pacific and Atlantic Oceans (Diaz et al., 1998; Doyle and Barros, 2002; Berri and Bertossa, 2004) and by moisture flux from tropical South America (Rodrigues and Cavalcanti, 2006; Zamboni et al., 2010).

The LPB region presents different climate regimes in the northern and southern sectors (Berbery and Collini, 2000; Rodrigues and Cavalcanti, 2006). The northern region presents a well-defined annual cycle of precipitation: the tropical South America regime, with large amounts of rainfall during the summer, associated with the South Atlantic Convergence Zone (SACZ) (Kodama, 1992), and with minimum precipitation in the winter (Berbery and Barros, 2002). These features are consistent with the South America Monsoon System (SAMS) regime and have been discussed in the review studies of Vera et al. (2006) and Marengo et al. (2012), among other studies. The influence of intraseasonal climate variability on precipitation anomalies in the SACZ was shown in Nogués-Paegle and Mo (1997), Carvalho et al. (2004) and Cunningham and Cavalcanti (2006) and the submonthly activity of the SACZ was discussed by Liebmann et al. (1999). On the other hand, the southern sector presents uniform precipitation throughout the year, registering a lower amount of monthly rainfall than that registered over the northern portion (Rodrigues and Cavalcanti, 2006). The southern region is affected mainly by transient systems associated with cold fronts (Cavalcanti and Kayano, 1999; Vera et al., 2002) and by mesoscale convective systems (Velasco and Fritsch, 1987; Salio et al., 2007).

Positive precipitation trends over La Plata Basin in the second half of 20th century have been discussed by several researchers, such as Berbery et al. (2006), Boulanger et al. (2005) and Penalba and Vargas (2004). An increase in the number of precipitation extremes over the region has been documented by Berbery et al. (2006) and Re and Barros (2009), with the largest precipitation increase observed in southern Brazil and northeastern Argentina climatologies, from November to May.

Extreme precipitation events over La Plata Basin have been associated with El Niño-Southern Oscillation (ENSO) conditions, which affect the region mainly from spring until the following winter, with occurrence of droughts or floods. In El Niño years, above-normal precipitation occurs over the region, leading to floods and river overflows (Kousky et al., 1984; Camilloni and Barros, 2003; Chamorro, 2006; Grimm et al., 1998). During La Niña, dry conditions are observed in the region, bringing shortage of water and problems in agriculture and cattle management (Grimm et al., 2000). The El Niño episode of 1982/1983 was one of the strongest of the 20th century and caused large damage in southern Brazil, Paraguay, Uruguay, and Argentina (Kousky et al., 1984). The flooding of the Paraguay River affected millions of people, destroying houses and public buildings, with serious consequences to cattle-raising and agriculture (Chamorro, 2006). Social and economic impacts of flooding in 1982/1983, 1992 and 1997/1998 were documented by Chamorro (2006). In Paraguay more than 60,000 people were affected by El Niño related floodings in 1982/1983, more than 70,000 in 1992, and more than 80,000 in the interior and about 25,000 in Asuncion in 1997/1998.

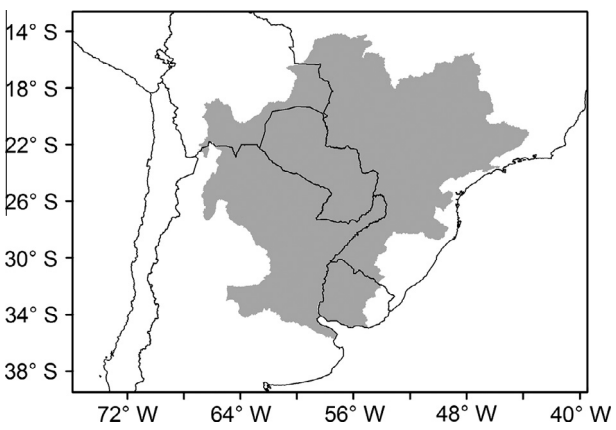

Fig. 1. La Plata Basin in South America.

River discharges associated with events of extreme precipitation over La Plata Basin were discussed by Berbery et al. (2006). The authors suggested that a 1% increase of precipitation leads to a 2% increase in the river discharge and found that the largest monthly discharge events in Uruguay River occur during El Niño episodes. Above average precipitation over Uruguay in El Niño years was identified by Pisciottano et al. (1994). Grimm and Tedeschi (2009) assessed the influence of ENSO on the frequency and intensity of extreme precipitation events in South America for each month of the ENSO cycle, based on a large set of daily station rainfall data, and compared the results with the influence of ENSO on the monthly total rainfall. Significant ENSO signals in the frequency of extreme events were found over extensive regions of South America during different periods of the ENSO cycle. Different types of ENSO (i.e. canonical vs central, Kug et al., 2009) affect extreme precipitation events over South America in different ways (Tedeschi et al., 2014): There is a greater increase (decrease) of extreme events in the southeastern South America, including LPB (tropical) during East El Niño than in Central El Niño, when compared to normal years. The influence of Pacific SST on extreme precipitation over southeastern Brazil was also identified by Liebmann et al. (2001).

Focusing on extreme rainfall in the LPB region, Robledo et al. (2013) described the main patterns of co-variability between monthly means of daily intensity of extreme rainfall in Argentina and global SST anomalies for spring, summer and autumn. They show that positive SST anomalies in the tropical Pacific, mainly related to ENSO activity, are associated with increased extreme daily rainfall in central and northeastern Argentina. In addition, they found significant relationship between extreme rainfall anomalies and SST anomalies in other tropical oceans, like tropical Indian and Atlantic Oceans.

Some extreme events occur during neutral ENSO years and may be associated with other large-scale features, such as the Antarctic Oscillation or Southern Annular Mode (Silvestre and Vera, 2003; Vasconcellos and Cavalcanti, 2010; Menéndez and Carril, 2010), blocking situations (Mendes et al., 2008), and South Atlantic SST influence (Doyle and Barros, 2002; Diaz et al., 1998; Barros et al., 2000). Specific synoptic and mesoscale systems are responsible for daily extremes, such as the flooding episodes that occurred over Argentina at the end of March and at the beginning of April 2007 (Cavalcanti, 2012). Around 50,000 people were evacuated from their houses and towns in central-west Argentina because of the heavy rainfall in the region, which caused floods and high river discharges. Thirteen people died during the episode, which lasted seven days, and several places were isolated because of fallen bridges and flooding of roads. Three million hectares in the region, highly productive in agriculture and cattle-raising were submersed, affecting the food production. Moreover, the risk of infection increased after the episode. Southern and western Uruguay were also affected by heavy rains during this period, with 800 people reported to have been evacuated from their homes. Other extreme wet and dry events that occurred in the first decade of 21st century are discussed in Cavalcanti (2012).

With the evidence of precipitation increase over La Plata Basin during the 20th century, as mentioned above, and also discussed in Liebmann et al. (2004), it is important to analyze future scenarios of climate change, to verify whether this trend is expected to continue and at what rate, and also whether this increase is associated with the trend in extreme precipitation events. There is a need to know not only the frequency of episodes but also the intensity and the associated mechanisms, in order to provide reliable information that can be used for mitigation and adaptation to reduce the impacts. It is also important to analyze the influence of climate change superimposed on natural climate variability. Much of the precipitation over the La Plata region is related to the moisture transport from the Amazon region, and changes due to Amazonia deforestation or increase of greenhouse gases will affect the precipitation and hydrological cycle over La Plata Basin. The SST increases in the Pacific and Atlantic Oceans in future climate may also affect the precipitation over the region, due to the influence that these oceans have on South American climate.

Results from several models of the Coupled Model Intercomparison Project Phase 3 (CMIP3) and Coupled Model Intercomparison Project Phase 5 (CMIP5) showed a precipitation increase over the La Plata Basin region in the future climate (Jones and Carvalho, 2013; Cavalcanti et al., 2006; Menéndez and Carril, 2010; Cavalcanti and Shimizu, 2012; Barros et al., 2013). Using a CMIP5 multi-model ensemble, Penalba and Rivera (2013) analyzed the future changes in drought characteristics over southern South America, obtaining that the occurrence of droughts will be more frequent during the 21st century, with shorter durations and greater severities. Regional climate models also projected a precipitation increase over LPB (Marengo et al., 2011). This increase can be attributed to higher extreme monthly precipitation as a consequence of an increase in the water vapor convergence in the lower atmosphere over the eastern LPB (Barros et al., 2013).

A collaboration project of a network involving Europe and South America (Climate Change Assessment and Regional Impact Studies in La Plata Basin (CLARIS-LPB Project), was created to study the climate change impacts on La Plata Basin and to design strategies of adaptation for land use, agriculture, rural development of hydropower production, river transportation, water resources, and ecological systems in wetlands. This project derived from the previous CLARIS project (Boulanger et al., 2010). The objective of one of the work-packages, "Processes and future evolution of extreme climate events in La Plata Basin," was to elucidate the climate processes associated with extreme hydroclimate conditions over the LPB region, considering the role of the large-scale forcing and the local interactions as well as the way in which the frequency and intensity of such cases may change according to different projections of global climate change. Knowledge of extreme precipitation frequency in the present climate and the projections for the future can provide useful information to the agriculture and hydrology sectors. The association of extremes with large-scale atmospheric and oceanic behavior, as well as with synoptic and mesoscale conditions, will improve the ability to monitor them.

Present climate conditions in the framework of the CLARIS and CLARIS-LPB EU projects have been analyzed by Menéndez et al. (2010a, 2010b), Solman et al. (2013) and Carril et al. (2012). Solman et al. (2013) found that CLARIS-LPB regional climate models reproduce well the spatial distribution of seasonal precipitation and that the intermodel spread is small over most of South America, except over the Andes region. Moreover, the ensemble mean appropriately reproduces the annual cycle of precipitation over vast regions of South America. Carril et al. (2012) analyzed a set of four regional models that were integrated for the period 1991–2000, over a continental-scale domain, driven by ERA40 reanalysis. The range of variability of strong precipitation events was analyzed within different subregions of southern South America. These strong events were defined as days when precipitation was above the 75th percentile. In most cases, individual models and the ensemble, systematically underestimated the intensity of events derived from gauge data. The comparison of model-simulated precipitation extremes with station-based observations has two main sources of uncertainty: the sparseness of the observing network over most of South America and the fact that models simulate grid box averages whereas observations are point values. Carril et al. (2012) showed that the models used within CLARIS were able to reproduce the broad spatial pattern of precipitation but they overestimated the convective precipitation in the tropics and the orographic precipitation over highlands, while underestimating both the precipitation near the monsoon core region and the daily intensity of rainfall over the whole domain.

In order to better understand the occurrence of extreme precipitation (wet and dry conditions) over LPB associated with large scale and local features, additional observational and modeling studies are presented in this article. The CLARIS-LPB Project allowed the collaboration among researchers of several institutions in South America and Europe and provided observed data and regional model outputs. In particular, specific purposes were (i) to investigate the influence of remote (i.e. Pacific, Indian and Atlantic Oceans SST) versus local (i.e. soil moisture) forcing on the characteristics of the precipitation extremes over LPB and (ii) to provide statistics of common used indices for wet and dry extremes over the region.

This study is organized as follows: Section 2 describes the data, the models used and the methods implemented to identify extremes. Section 3 collects the results on the influences of Pacific, Atlantic and Indian Oceans SST on extreme precipitation over LPB, considering both observations (Section 3.1) and models experiments results (Section 3.2). In particular, in the observed record, large-scale features are analyzed during extreme precipitation over two sectors of LPB in January because this is the peak of the summer season when droughts or flooding can have the largest impacts on the region (Section 3.1.1), and the influence of different types of ENSO is discussed as well (Section 3.1.2). Then climate simulations and projections are used to analyze the influence of ENSO episodes on the frequency of extreme precipitation events in LPB in the future climate (Section 3.2.1), and a specific set of model experiments is performed and analyzed to evaluate the sensitivity of SST forcing in different oceans affecting the extremes (Section 3.2.2). Section 4 is dedicated to the impact of local features (i.e. the soil moisture) on LPB precipitation in the observations (Section 4.1) and in regional models experiments (Section 4.2). Section 5 provides indices of wet and dry conditions in LPB, with emphasis on (i) the frequency and interannual variability of droughts in LPB using a monthly precipitation index (SPI) in Section 5.1; (ii) future changes of dry spells based on daily climate indices projected by a set of regional models in Section 5.2; (iii) daily intensity extreme precipitation index over LPB and correlations with large-scale climate indices are presented in Section 5.3 and (iv) the frequency of monthly wet and dry extremes over two sectors of LPB analyzed with the SPI in the observations and in projections of global coupled models in Section 5.4. Finally, Section 6 presents the main conclusions.

2. Description of data, models used and definition of precipitation extremes

2.1. Observations

Observed precipitation and temperature data are obtained from CLARIS station database (Penalba et al., 2014) used in Sections 4.1, 5.1 and 5.3. Other precipitation datasets include the gridded

1° × 1° daily precipitation for the period 1956–2002 from stations over South America (Grimm and Tedeschi, 2009), used in Sections 3.1.2 and 3.2.1, and monthly precipitation data at resolution 2.5° × 2.5° for the period 1979–2001 taken from the Global Precipitation Climatology Project (GPCP, Adler et al., 2003), used in Sections 3.1.1 and 5.4. The Extended Reconstructed Sea Surface Temperature (SST) database at resolution 2° × 2° for the period 1960–2008 (NOAA ERSST V3, Smith et al., 2008) is used in Section 3.1.2 and HadISST data at resolution 1° × 1° for the period 1960–2000 (Rayner et al., 2003) is used in Section 3.2.1. Atmospheric data are taken from the ERA 40 reanalysis, with a resolution of 1.125° × 1.125° for the period 1979–2001 (Uppala et al., 2005) and they are mostly used in Section 3.1.1.

2.2. Model outputs

Different models and type of experiments have been used in this study. The global models are CPTEC/INPE Atmospheric Global Circulation Model at resolution T62 L28 (Cavalcanti et al., 2002) and HadCM3 atmosphere–ocean coupled model from CMIP3, resolution 2.5° lat × 3.75° lon, L19 (Gordon et al., 2000) analyzed in Section 5.4. ECHAM4 atmospheric general circulation model (Roeckner et al., 1996) at T106 horizontal resolution and 19 sigma vertical levels is used in Section 3.2.1 and ECHAM5/MPI-OM [atmospheric resolution of T63 L31 described in Roeckner and Coauthors (2003) and ocean resolution of 1.5° and 40 vertical levels described in Marsland et al. (2003)], in Section 3.2.2. The scenario A2 is considered for the projections of global HadCM3 and ECHAM5/MPI-OM models.

The regional climate models used in the framework of the CLARIS-LPB Project are RCA (Samuelsson et al., 2011), PROMES (Sánchez et al., 2004), LMDZ (Hourdin et al., 2006), RegCM3 (da Rocha et al., 2009), MM5 (Solman and Pessacg, 2012), Eta (Chou et al., 2012) and REMO (Jacob et al., 2012). Results of these models are analyzed in Section 5.2. The regional models were integrated with 50 km of horizontal resolution over the South American domain. The RCMs forced by ERA-Interim reanalysis were integrated during the period of 1990–2008 for evaluation of the models (Solman et al., 2013) in a procedure consistent with CORDEX (COrdinated Regional climate Downscaling Experiments (Giorgi et al. 2009), http://wcrp.ipsl.jussieu.fr/SF_RCD_CORDEX.html). The integrations to assess the climate changes under global warming were performed over two 30-year periods: climate of the 20thcentury, as defined by CMIP3: (1960–1990) and distant future (2070–2100). PROMES, MM5, and ETA models are forced by the HadCM3 coupled general circulation model (CGCM); LMDZ model is forced by IPSL CGCM; and RCA, REMO and RegCM3 models are forced by ECHAM5 CGCM. All global models for the downscaling were obtained from the CMIP3 integrations of present time and future projections with scenario A1B (Nakicenovic and Coauthors, 2000).

2.3. Definition of precipitation extremes

The monthly extremes used in Sections 3.1.1, 5.1 and 5.4 are identified using the Standardized Precipitation Index (SPI) proposed by McKee et al. (1993). This index quantifies the number of standard deviations that the accumulated precipitation on a given time scale deviates from the average value of a location during a particular period. It identifies extreme wet/dry (SPI $\geqslant$ 2.0/SPI<=−2.0), severe wet/dry (1.5 $\leqslant$ SPI < 2.0)/(−2 < SPI $\leqslant$ −1.5), and moderate wet/dry (1.0 $\leqslant$ SPI < 1.5)/(−1.5 < SPI $\leqslant$ −1.0) conditions. The SPI index has been used to analyze droughts and above mean precipitation (Heim, 2002; Hayes et al., 1999). The Drought Hazard Index (DHI), proposed by Shahid and Behrawan (2008), is used in Section 5.1. This is a weighted index based on drought frequencies, which was constructed as a sum of drought classes with a weighting scheme, defined as the following expression: DHI = (MDr ×MDw) + (SDr × SDw) + (EDr × EDw). MD, SD and ED are moderate, severe and extreme drought classes; sub-index *w* represents the weight of the selected classes and sub-index *r* indicates the rating of the percentage of occurrences. The values of the weights and ratings can be found in Shahid and Behrawan (2008).

Extreme daily precipitation events are defined as cases where the precipitation is above a threshold of percentile 90 [Sections 3.1.2 and 3.2.1] and percentile 75 [Section 3.2.2]. In Section 4.1 an event is considered as extreme when the precipitation is lesser (greater) than its 10th (90th) percentile. The precipitation threshold for defining humid days (Sections 3.2.2 and 4.2) and dry days (Section 5.2) is 1 mm/day (Kjellström et al., 2010). In Section 5.3 the intensity of daily extreme rainfall (DIER) is calculated as the ratio between the monthly-accumulated extreme rainfall and the number of days with extreme precipitation (higher than 75th daily percentile) events per month. A detailed description of the methods used is given in each sub-section where of interest.

3. Precipitation extremes over LPB and large scale influences

In this section, large-scale influences such as teleconnections, influences of Pacific, Indian and Atlantic SSTs on extreme precipitation over LPB are discussed in observational data and model experiments. Modoki-type ENSO is contrasted with the Canonical ENSO. The extremes related to ENSO under a future global warming scenario are identified in model simulations and projections.

3.1. Observations

3.1.1. Pacific-Indian region features associated with extreme precipitation in two sectors of LPB in January

The LPB region extends from subtropical to extratropical latitudes of South America (Berbery and Barros, 2002). Therefore, to analyze the events of extreme monthly precipitation, one must divide the region in different sectors, because of the different precipitation regimes. Here the extremes are analyzed in the northern (15°S–25°S; 55°W–45°W) and the southern (25°S–35°S; 60°W–50°W) sectors of LPB (Fig. 1). January, the peak of the austral summer season, is a month with large extreme precipitation events in the northern sector, mainly because of SACZ occurrences and features of the South American Monsoon System (Marengo et al., 2012) and references therein. Extreme, severe, and moderate cases obtained from SPI are analyzed in composites of wet and dry cases in the northern and southern LPB sectors.

Anomaly precipitation composites for wet January events in the northern (southern) LPB are shown in Fig. 2a and b. The composites of both sectors display the precipitation dipole over South America associated with the SACZ characteristics (Nogués-Paegle and Mo, 1997; Carvalho et al., 2002; Cunningham and Cavalcanti, 2006; Robertson and Mechoso, 2000). When wet conditions occur in the northern sector, these are mostly related to SACZ occurrences, and drier conditions affect the southern sector. The opposite occurs when wet conditions characterize the southern sector. This precipitation dipole is a very robust signal of SACZ variability, and it is found at several timescales, from submonthly [Liebmann et al., 1999; Carvalho et al., 2002], intraseasonal [Nogués-Paegle and Mo, 1997; Nogués-Paegle et al., 2000; Carvalho et al., 2004; Cunningham and Cavalcanti, 2006] to interannual [Vasconcellos and Cavalcanti, 2010; Junquas et al., 2012; Robertson and Mechoso, 2000]. Mechanisms responsible for this dipole have been related to wavetrains from the Pacific Ocean, and moist flux from the Amazon basin may contribute as well to precipitation extremes in LPB (Silva and Berbery, 2006).

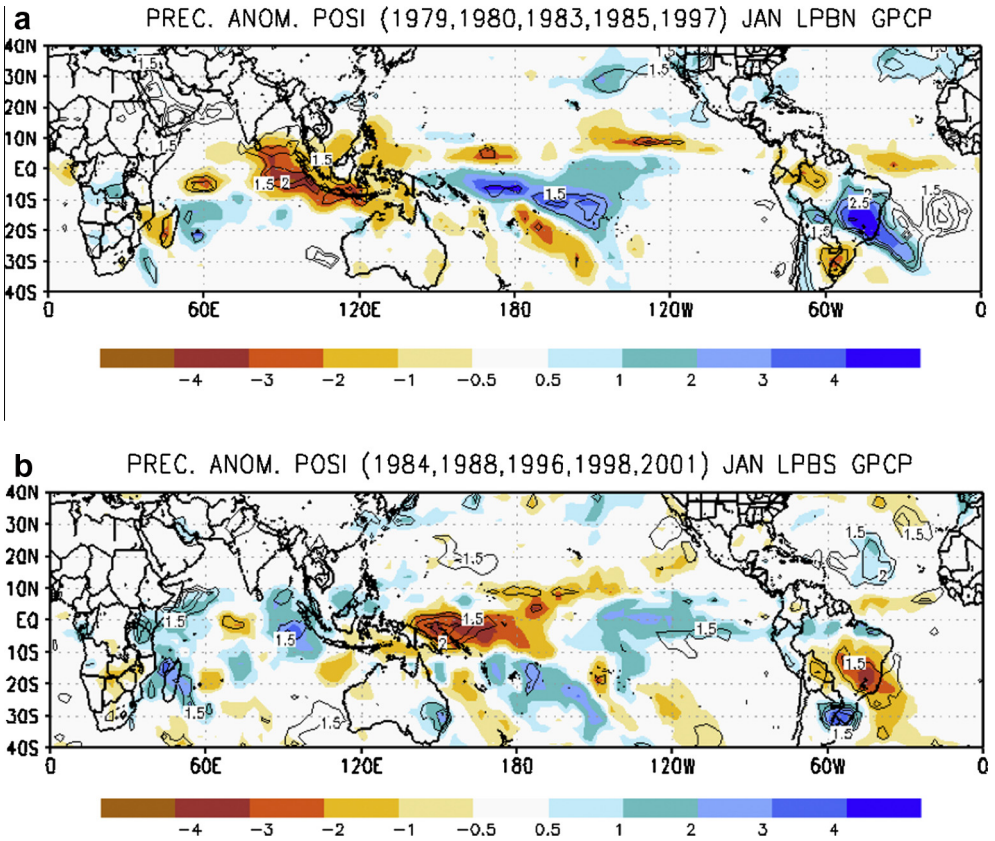

Fig. 2. GPCP anomaly precipitation of wet extremes composites over (a) the northern and (b) the southern sectors of LPB during January. Contours above 1.5 show regions with significance higher than 90%.

Fig. 2 shows that in the cases of precipitation extremes in northern and southern LPB, there is also a north–south dipole of precipitation over the western South Pacific and a west-east dipole between equatorial eastern Indian Ocean and western Pacific. These dipoles invert signs, from the northern sector extremes composites to the southern sector extremes composites, following the dipole inversion over South America. Composites of geopotential anomalies show the existence of wavetrains from the western tropical Pacific to South America (PSA-type) in the wet cases of the northern sector (Fig. 3a), when the precipitation (and convection) anomaly is positive in the western Pacific equatorial region (Fig. 2a). For the southern sector, the wavetrain that reaches South America starts over the Indian Ocean (Fig. 3b), when there is a positive precipitation anomaly over the Indian Ocean (Fig. 2b). Influences of wavetrains from the Indian Ocean toward Southern Atlantic Ocean on South America were also discussed in Saji and Yamagata (2003), Saji et al. (2005), Chan et al. (2008) and Taschetto and Ambrizzi (2012).

3.1.2. Impact of canonical and Modoki-type ENSO on extreme precipitation over LPB

As mentioned in the introduction, ENSO affects extreme precipitation over LPB. Taking into account that seasonal precipitation anomalies over South America display different results for two types of ENSO (Tedeschi et al., 2013), in this sub-section precipitation extremes are analyzed for cases of these two types.

Following the method used by Grimm and Tedeschi (2009), the Gamma distribution (Thom, 1958) for each day of the year is used to define the extreme precipitation events as three-day running means of percentile greater than 90th. For the evaluation of the impact, two types of ENSO have been considered (Tedeschi et al., 2013): the canonical ENSO (SST anomalies in the tropical eastern Pacific) and the ENSO Modoki + A (Modoki criterion + central Pacific SST anomalies greater (less) than $0.7\sigma_A$ ($-0.7\sigma_A$), where σ_A is the SSTA standard deviation of area A). The Modoki criterion follows the Modoki index defined by Ashok et al. (2007): EMI = $[SSTA]_A - 0.5^* [SSTA]_B - 0.5^* [SSTA]_C$ The brackets represent the area-averaged SSTA (SST anomaly) over each region: A (165°E–140°W, 10°S–10°N), B (110°W–70°W, 15°S–5°N), and C (125°E–145°E, 10°S–20°N).

During the spring season (September, October and November), when there are significant ENSO impacts over LPB, Canonical ENSO and ENSO Modoki + A show different results. The impact of these two types of ENSO on wet extremes over LPB, during this season, is shown in Fig. 4. During the analyzed period there are 8 years characterized as El Niño Canonical (ENC) and 6 years as El Niño Modoki + A (ENM). La Niña Canonical (LNC) occurred in 10 years and La Niña Modoki + A (LNM) in 2 years. The Canonical ENSO shows an increase (reduction) of extreme events in the LPB region during El Niño (La Niña). In the ENSO Modoki + A, however, a dipole between the northern and southern sector changes sign from El Niño to La Niña, indicating an increased number of wet extremes in the southern sector and reduction in the northern sector during El Niño, and the opposite during La Niña.

3.2. Model results

3.2.1. The impact of climate change on precipitation extremes over LPB in ENSO years

The most dramatic consequences of climate variability result from changes in extreme events. An ensemble of three model runs with ECHAM5/MPI-OM is analyzed to assess how models are able

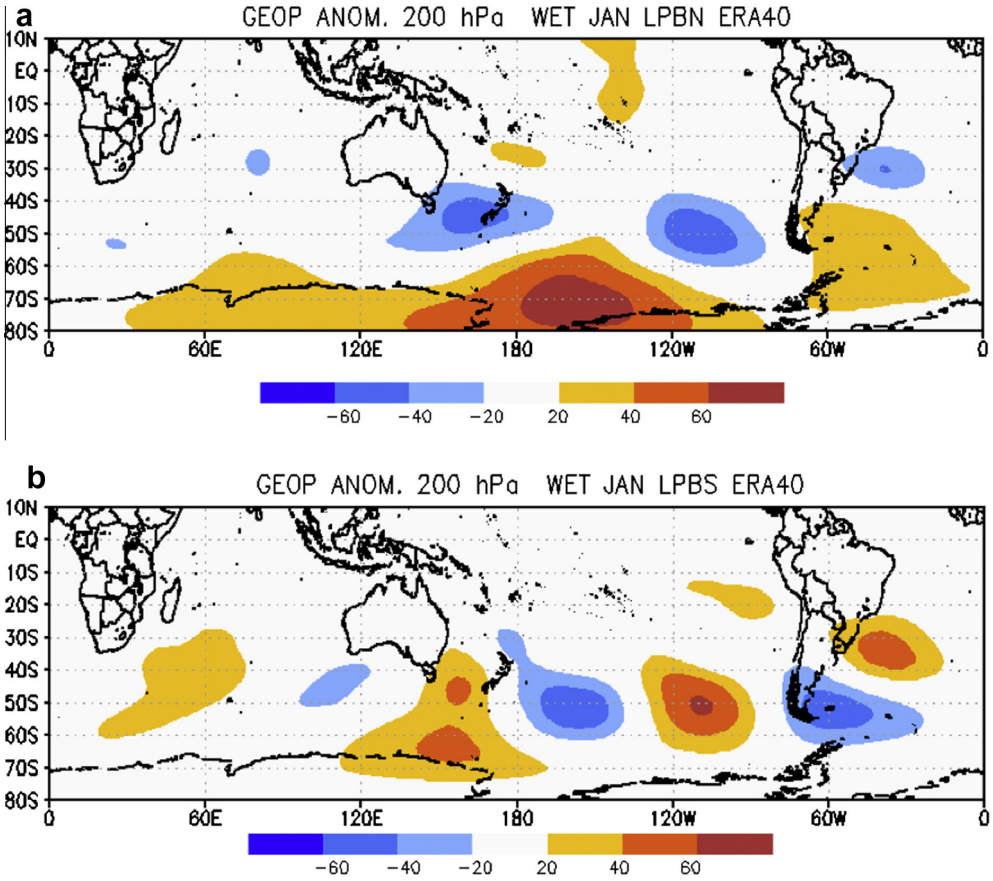

Fig. 3. ERA 40 geopotential anomaly at 200 hPa of wet extremes composites over (a) the northern and (b) the southern sectors of LPB during January.

to simulate the impact of ENSO on extreme rainfall in South America. Results of climate simulations are compared to observations for the period 1960–2000. Then the projections of future climate under emission scenario A2 (2060–2100) are analyzed. The criterion to select the extremes is the same as in the previous sub-section. ECHAM5 was chosen due to the good performance in reproducing the La Plata Basin precipitation climatology (Grimm, 2011) and because it simulates ENSO reasonably well (Grimm and Natori, 2006).

Fig. 5 shows the first mode of SST variability (related to ENSO) from observations and from ECHAM5-OM. The model shows the strongest anomalies shifted to the west and weaker opposite anomalies in the western Pacific and subtropical northern and southern Pacific. The El Niño (EN) and La Niña (LN) years are determined from the Niño 3 SST anomalies in both observations and model. Each EN (LN) episode must have at least six consecutive values of five months' running mean of a Niño 3 SST anomaly above (below) 0.5 °C (−0.5 °C). Here, two months for which previous studies indicated important ENSO impacts on La Plata Basin have been chosen for analysis: November (0) and April (+), where (0) indicates the year in which an episode starts and (+) indicates the following year (Grimm et al., 1998, 2000; Grimm, 2003, 2004). In November (0), the ENSO impact on La Plata Basin is stronger than in other months, in terms of relative precipitation intensity, while in austral autumn (+) some of the strongest ENSO-related floods occurred in the basin. These months are also those for which the model shows good performance in reproducing the ENSO impact (Grimm and Natori, 2006). In November (0), the model represents reasonably well the impact of El Niño on the frequency of extreme events in regions where November is part of the rainy season, but for few regions in western Amazon, although the impact is a little underestimated over southeastern South America (Fig. 6a and b).

Fig. 7a confirms that the model simulates the increased (reduced) frequency of extreme events observed over southern Brazil during El Niño (La Niña) episodes (as shown in Grimm and Tedeschi, 2009). In the projected climate for A2 future scenario, the impact of ENSO on extreme events increases (Fig. 6c), as confirmed by Fig. 7b. The strong impact of El Niño episodes on the frequency of extreme events in La Plata Basin in April (+) is well reproduced by the model and this impact is also strengthened in the future climate scenario (not shown). The changes are significant in southern Brazil, as shown in Fig. 6b for El Niño. For La Niña the difference in southern Brazil is also significant, as shown in Grimm and Tedeschi (2009). These are gamma distributions, which fit well on daily precipitation.

The increase of extreme events during El Niño in La Plata Basin does not necessarily mean that the El Niño impact will be stronger in the region in a future scenario of enhanced content of greenhouse gases, in terms of monthly or seasonal precipitation anomalies, since the increase of the frequency of extreme precipitation is accompanied by the reduction of the frequency of weak or moderate daily precipitation (Fig. 7b). Rather, it means that the number of extreme events will increase, since the difference between the frequency of extreme events in the future and the present climate is positive in the region for all categories of years (El Niño, La Niña, and neutral, figures not shown). This is coherent with the conclusions of Trenberth (2011) that in a scenario of enhanced greenhouse gases concentrations and global warming, the frequency of more intense precipitation would increase. However, La Niña episodes will still produce fewer extreme events in the region than El Niño events, as in the present climate.

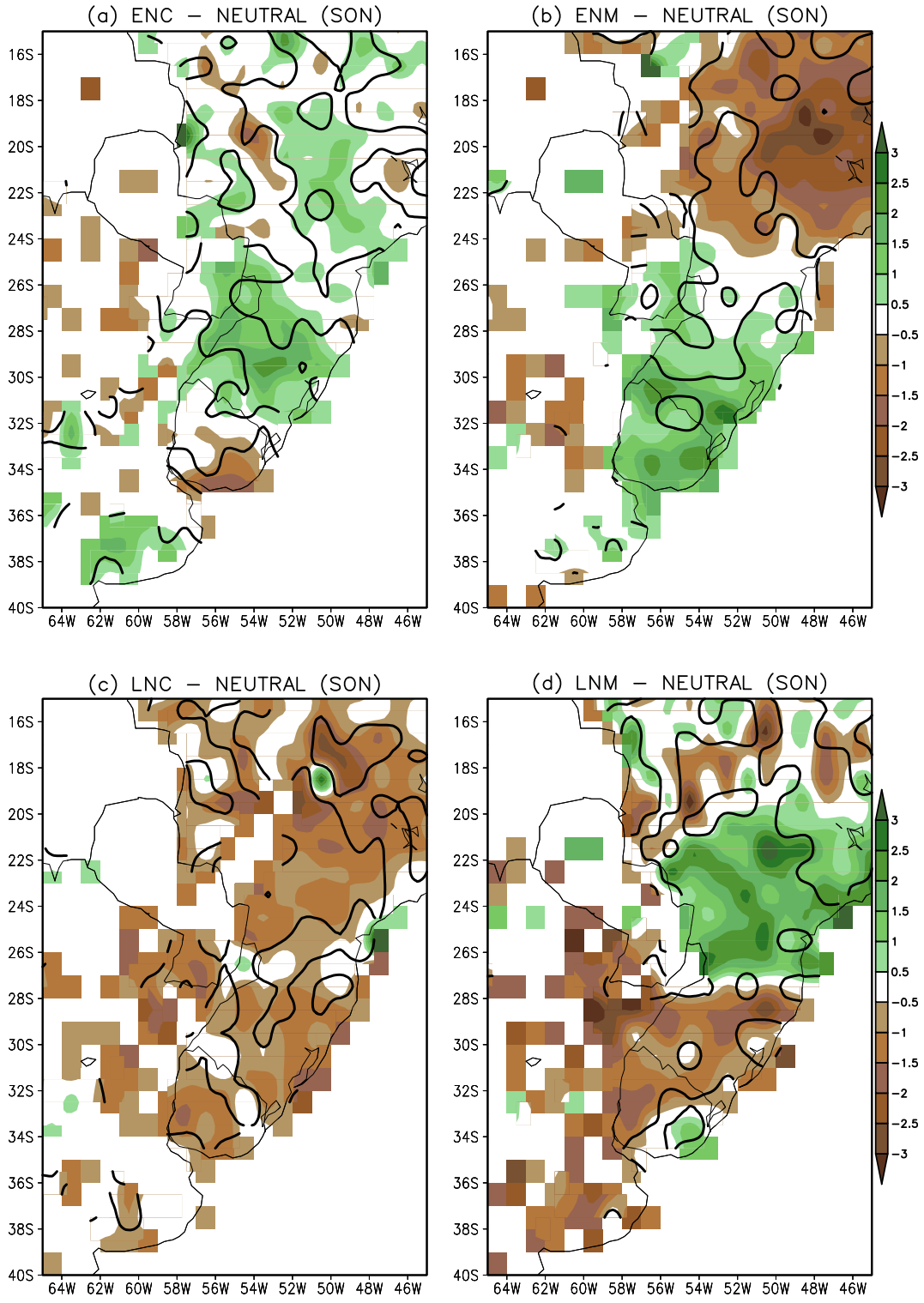

Fig. 4. Differences between observed numbers of extreme precipitation events in ENSO years and neutral years, for SON (a) Canonical El Niño and (c) La Niña episodes and (b) El Nino Modoki + A and (d) La Nina Modoki + A. Colors indicate the difference and the gray lines limit the areas where the differences are significant over the 90% confidence level.

3.2.2. Pacific, Indian and Atlantic Oceans SST influences on LPB precipitation extremes: Sensitivity experiments

SST-forced experiments are performed to illustrate how the large-scale patterns that modulate the interannual hydroclimate variability over LPB in spring emerge not only from tropical Pacific SST, but also from tropical Atlantic and Indian Oceans SST forcing. Spring was chosen because in this season ENSO impacts are large over LPB and also because of the maximum lagged cross-correlation between the tropical north Atlantic and ENSO SST anomalies (Wang, 2002). The analysis of two regions in the Pacific sector is chosen to account for the shift in behavior, frequency and characteristic of El Niño that occurred in recent decades (e.g. Ashok and

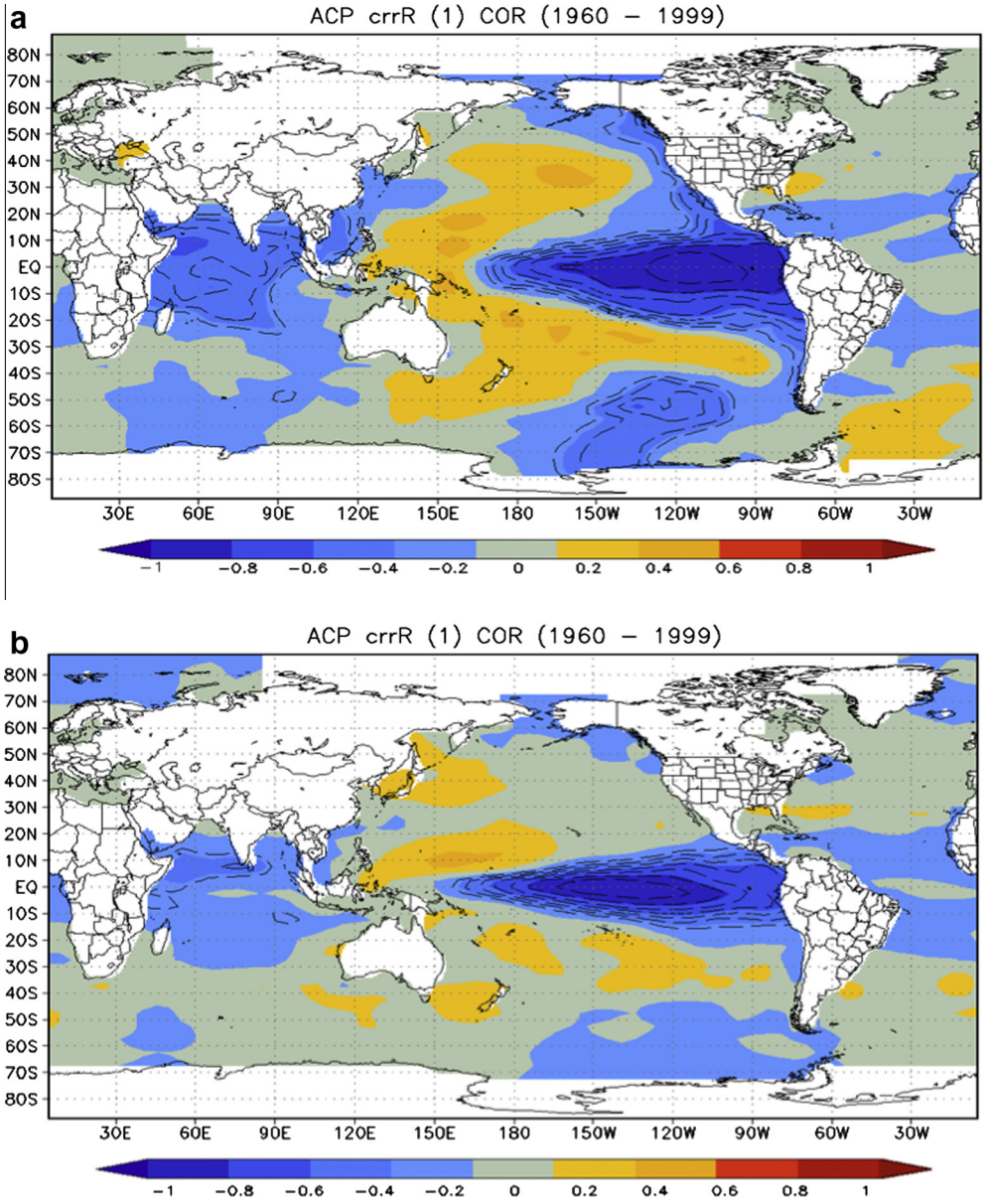

Fig. 5. First EOF factor loadings of (a) observed SST from HadISST and (b) SST simulated by ECHAM5-OM, for the period 1960–2000.

Yamagata, 2009; Yeh et al., 2009). Different positions of SST anomalies in the Pacific Ocean have different impacts on precipitation extremes over LPB, as shown in Section 3.1.2 and also in Tedeschi et al. (2014).

Using the same model as in Cherchi et al. (2014) (ECHAM4; see their Section 2 for details on the model), five 35-year long experiments are performed: one control run (CTRL), in which the model is forced with climatological SSTs, and four sensitivity experiments in which positive SST anomalies are superimposed to the climatology over the eastern Pacific (EPac; a warm pool centred at 0°, 100°W), the central Pacific (DPac; 0°, 175°W), the central Indian (CInd; 0°, 70°E) and the tropical North Atlantic (NAtl; 15°N, 20°W) Oceans respectively. The SST anomalies are turned on from June to February for the Indo-Pacific experiments (EPac, DPac and CInd), but lagged by about 5 months for the NAtl experiment.

This analysis focuses over LPB during the late austral spring (October–November), when the regional interannual standard deviation of daily precipitation maximizes (not shown). To investigate the effects on precipitation extremes, differences in percentiles' thresholds and anomalies in the frequency of days exceeding those thresholds are analyzed.

When warm SST anomalies are placed in central Pacific, central Indian and tropical North Atlantic oceans there is a reduction of the mean precipitation over vast areas in LPB (Fig. 8a–c). The EPac experiment represents an exception, as relatively wet mean conditions are favored (Fig. 8d). Nevertheless, because the statistical distribution of daily precipitation has positive skewness (not shown) the mean is not the most frequent value and it is sensitive to extreme values in the right tail. When considering the sensitivity to the 75 percentile threshold (P75), the signal over LPB is still negative for DPac, CInd and NAtl experiments (Fig. 8e–g), but the anomalies as well as the area centered in LPB and affected by negative anomalies are larger. Results suggest that warm SST anomalies in the corresponding oceans favor regional negative anomalies in precipitation that could be partially explained by changes in extremes. In the EPac experiment, the differences with the CTRL are small but positive, indicating an increase of the P75 threshold (Fig. 8h).

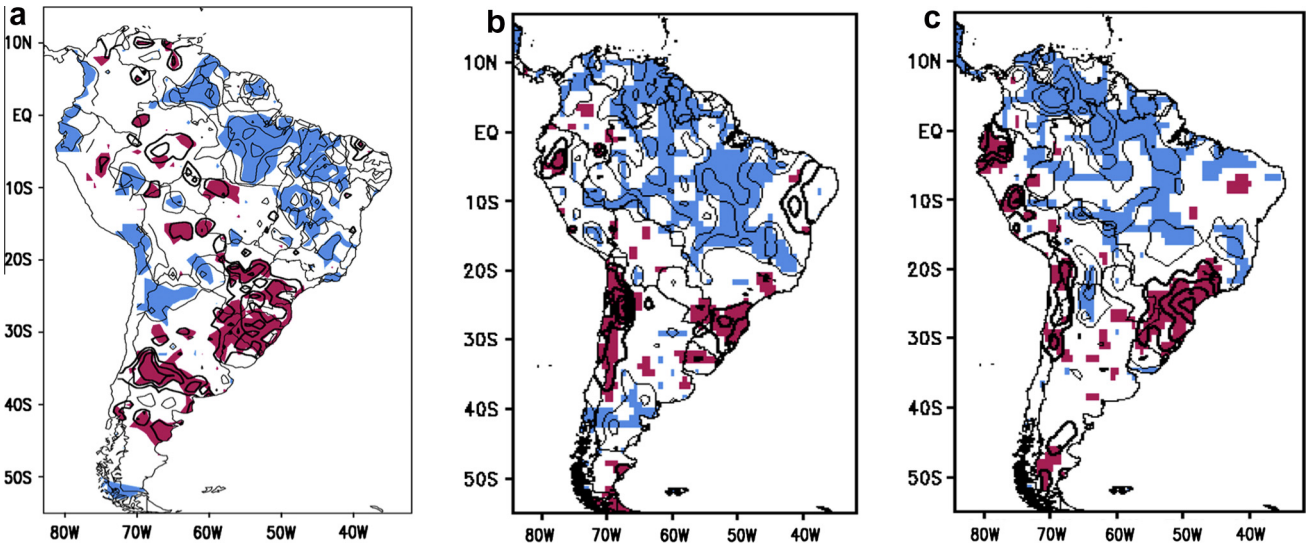

Fig. 6. Differences between average numbers of extreme events in November (0) of El Niño years and neutral years in (a) observations, (b) simulations by the coupled model ECHAM5-OM in the twentieth century climate (1960–2000), and (c) projections of future climate, under emission scenario A2 (2060–2100). Regions in red (blue) present positive (negative) differences with level of significance between 0.0 and 0.10.

The sensitivity of the number of days with heavy precipitation (i.e., the number of days in which precipitation is above the P75 threshold of CTRL) is shown as well in Fig. 8. When a positive SST anomaly is located in the tropical North Atlantic, central Indian and central Pacific oceans, the number of days with heavy precipitation over LPB decreases (Fig. 8i–k). On the contrary, in the EPac experiment, the small positive changes in the mean value could be explained by small increases in the frequency of occurrence of heavy precipitation days (at least in some LPB sub-regions; Fig. 8l). Precipitation frequency in the first quartile (i.e., the number of days with light precipitation defined as precipitation below P25 threshold of CTRL) presents little sensitivity to the SST forcing (not shown).

4. Feedbacks between soil moisture and precipitation in LPB

Besides remote influences on precipitation extremes, as shown in the previous section, local features can also contribute to extreme anomalies in LPB rainfall. In this section, feedbacks between extreme precipitation and extreme soil moisture conditions, as well as the influence of soil moisture feedbacks on precipitation in model experiments are discussed.

4.1. Hydric conditions of the soil under extreme precipitation and potential evapotranspiration

LPB has large agricultural areas and therefore hydric conditions of the soil are essential for agriculture management. An agricultural dry condition occurs when water storage and rainfall are inadequate during the growing season. An evaluation of how hydric condition is sensitive to water and heat stress (low rainfall and high evapotranspiration) in the region is discussed. In order to evaluate these relationships, the probability of extremely unfavourable hydric condition associated to thermal or water stress is evaluated.

Observed precipitation and temperature data of 40 climatological stations in the argentine sector of La Plata Basin during the period 1970–2010 are used from CLARIS database (Penalba et al., 2014). Monthly Water Balance of the soil is calculated using the method proposed by Thornthwaite and Mather (1957) and Pascale and Damario (1977). Values of monthly potential evapotranspiration are estimated from Thornthwaite's method, modified by Camargo et al. (1999) using the effective capacity of soil water provided by Forte Lay and Spescha (2001).

The crops suffer hydric stress when the difference between precipitation and potential evapotranspiration is negative. As a result, the actual evapotranspiration is lesser than potential evapotranspiration. Deficit conditions in soil are computed as the difference between potential and actual evapotranspiration, following Pántano et al. (in press). On the other hand, when the precipitation is higher than the potential evapotranspiration and the water storage on soil reaches the field capacity, the surplus cause excess conditions. Under these considerations, the monthly hydric condition (HC) of the soil is estimated as the difference between excess minus deficit. From these terms, two monthly extreme unfavorable hydric conditions are evaluated: when there is high potential evapotranspiration (greater than 90th percentile) and when there is extreme low rainfall (less than 10th percentile).

For winter crops, April and July are two critical months in this region. The water recharge of the soil during April is crucial to let the crops handle the scarce precipitation occurring in the winter. Fig. 9 shows the spatial evaluation of these probabilities for April and July. During July, most of the stations with higher probability of extreme hydric condition under extreme high potential evapotranspiration are located west of 60°W and under extreme low rainfall eastward. During April, almost the whole region shows high values of probability of unfavourable hydric condition under both extreme low rainfall and extreme high potential evapotranspiration. Therefore, April is a risky month because extremely dry conditions with both high thermal stress and low water may severely impact the winter crops.

In order to analyze the temporal variability of these extreme conditions, the number of stations for April of each year that presented extreme potential evapotranspiration and extreme low rainfall (Fig. 10) is computed. During 1970, 1974, 1997, 2008 and 2009 almost the whole region (more than 26 stations, 65%) was under extreme potential evapotranspiration; and 1970, 1974, and 2008 presented more than 14 stations under extreme dry condition. Thus, the 1970s was the most affected decade, presenting

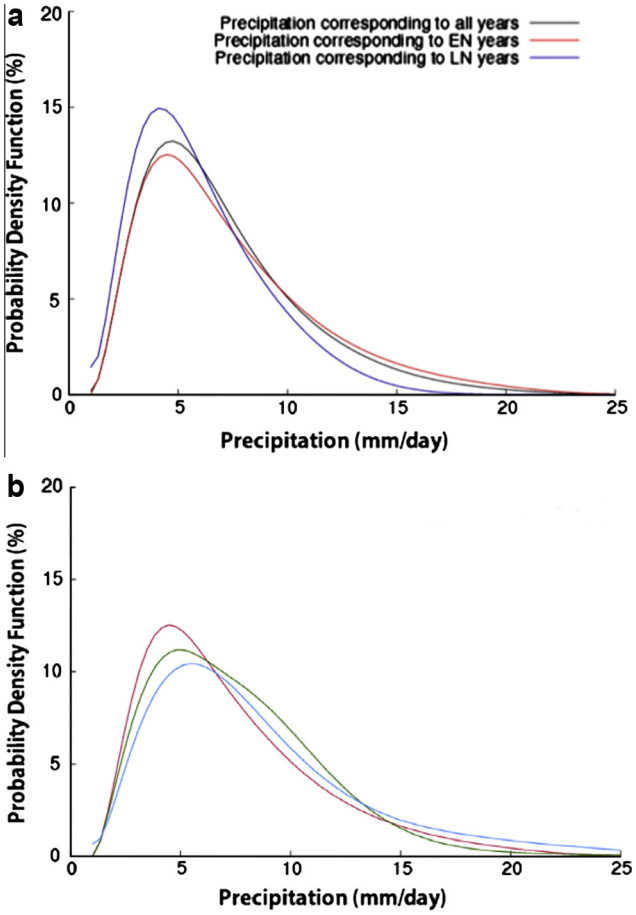

Fig. 7. (a) Probability density functions of daily precipitation over South Brazil simulated by ECHAM5-OM in the present climate (1960–2000) for November (0) of El Niño, La Niña and all years. (b) Probability density functions of daily precipitation over South Brazil, simulated by ECHAM5-OM in the present climate (1960–2000, pink line) and future scenario A2 (2060–2100, blue line) for November (0) of El Niño years. The green line is the distribution for the period 2060–2100, but with greenhouse gases concentration fixed at the value for 2000.

two years with more than 35% of the region under extreme conditions from both variables. A comparison between the mean hydric condition of this decade and its climatology, based on 1970–2010, shows that this decade presents values below normal for April (Fig. 11). It is shown that scarce water and heat stress contributed to the resulting dry decade.

4.2. Effects of soil moisture–atmosphere coupling on precipitation indices – Model experiments

The soil moisture is affected by precipitation, as seen in the previous sub-section, but it is also a source of humidity to the atmosphere, contributing to the precipitation in a feedback mechanism. In order to explore the impact of this feedback on different daily precipitation indices, model experiments are analyzed in this sub-section. A large portion of La Plata Basin has the potential to exhibit a strong land surface–atmosphere coupling during austral summer, compared with the rest of the continent (Sörensson and Menéndez, 2011). The coupling between soil moisture and evapotranspiration is particularly evident in the region (Ruscica et al., 2014).

The influence of inhibited soil moisture–atmosphere interaction on precipitation characteristics is studied through comparison of different precipitation indices, defined below. Because the values are from an ensemble of simulations, the mean length of consecutive wet days (MEC) and maximum length of consecutive wet days (MAC) indices are defined as the average of the indices of each individual member.

Experiments with the Rossby Centre Regional Climate model (RCA3) are performed for the austral summer of 1992/1993 to study the impact of soil moisture on extreme precipitation. This summer was selected for having neutral ENSO conditions. To describe the daily rainfall intensity, frequency of wet days and the length of wet spells, the following indices are used: (i) Mean daily intensity of precipitation (MIP) or mean rainfall per wet day (ii) Relative frequency of wet days (RF) calculated as the number of wet days divided by the total number of days, (iii) Mean length of consecutive wet days (MEC) and (iv) Maximum length of consecutive wet days (MAC). The threshold for a wet day is 1 mm. The methodology consists in comparing two ensembles of seasonal simulations performed with a regional climate model, one with two-way-interaction between soil moisture and atmosphere (ensemble W) and the other one with prescribed soil moisture (ensemble S), where the prescribed soil moisture field for each model time step is taken from one member of the ensemble W (similar to Koster et al., 2006). In other words, in ensemble S the soil moisture is a boundary condition for the atmosphere and may affect, for example, evapotranspiration or precipitation but the atmosphere will not affect soil moisture.

Fig. 12 shows the indices listed above, averaged in southeastern South America obtained from the ensemble W (panels a–d), and their differences between the ensembles W and S, expressed as a percentage of the values of W (panels e–h). The MIP index (Fig. 12a) shows a northwest-southeast band of maximum near 30°S. The spatial distribution of this index is similar to the 95th percentile of precipitation (not shown), and it is also worth noting that MIP has a rather different geographical distribution than the mean seasonal precipitation (the simulated seasonal mean has a south-north gradient with relative maxima over the Brazilian coast and along the eastern slope of the Andes, not shown). Regarding the RF index (Fig. 12b), the maximum values are found in the northern LPB (frequency greater than 50%) and the minimum over Uruguay (about 25%). The spatial distribution of the RF index is anticorrelated with the coupling between soil moisture and evapotranspiration as discussed in Ruscica et al. (2014), and it is similar to that of the MEC and MAC indices (Fig. 12c and d respectively).

In the area around Rio de la Plata, the model simulates no more than two mean and not more than five maximum consecutive wet days, while in the north of LPB, up to six mean and fifteen maximum consecutive wet days. In general, the maximum values of the MIP index in southeastern South America match minimum values of RF, MEC and MAC indices. Fig. 12e-h show the relative differences in the indices between the ensembles W and S. Positive values (red) indicate areas where inhibited soil moisture-atmosphere interactions decrease the indices. A negative gradient from west-southwest to east-northeast appears for all differences. This suggests that ensemble W has more (less) intense and frequent rainfall and longer wet periods than ensemble S in the western and southern (eastern and northeastern) sectors. Soil moisture can have local impacts through feedbacks with evapotranspiration and precipitation, as well as regional-scale impacts by affecting circulation patterns. In this experiment, it is found that the soil moisture from ensemble S is drier than the average soil moisture of the ensemble W in northern Argentina. A corresponding forced increase of the sensible heat flux and decrease of evapotranspiration induce a strengthened thermal low over this region in ensemble S that impacts the monsoon circulation in subtropical South America. The atmospheric moisture flux from the north in the area affected by the low level jet is weaker in the ensemble S. The

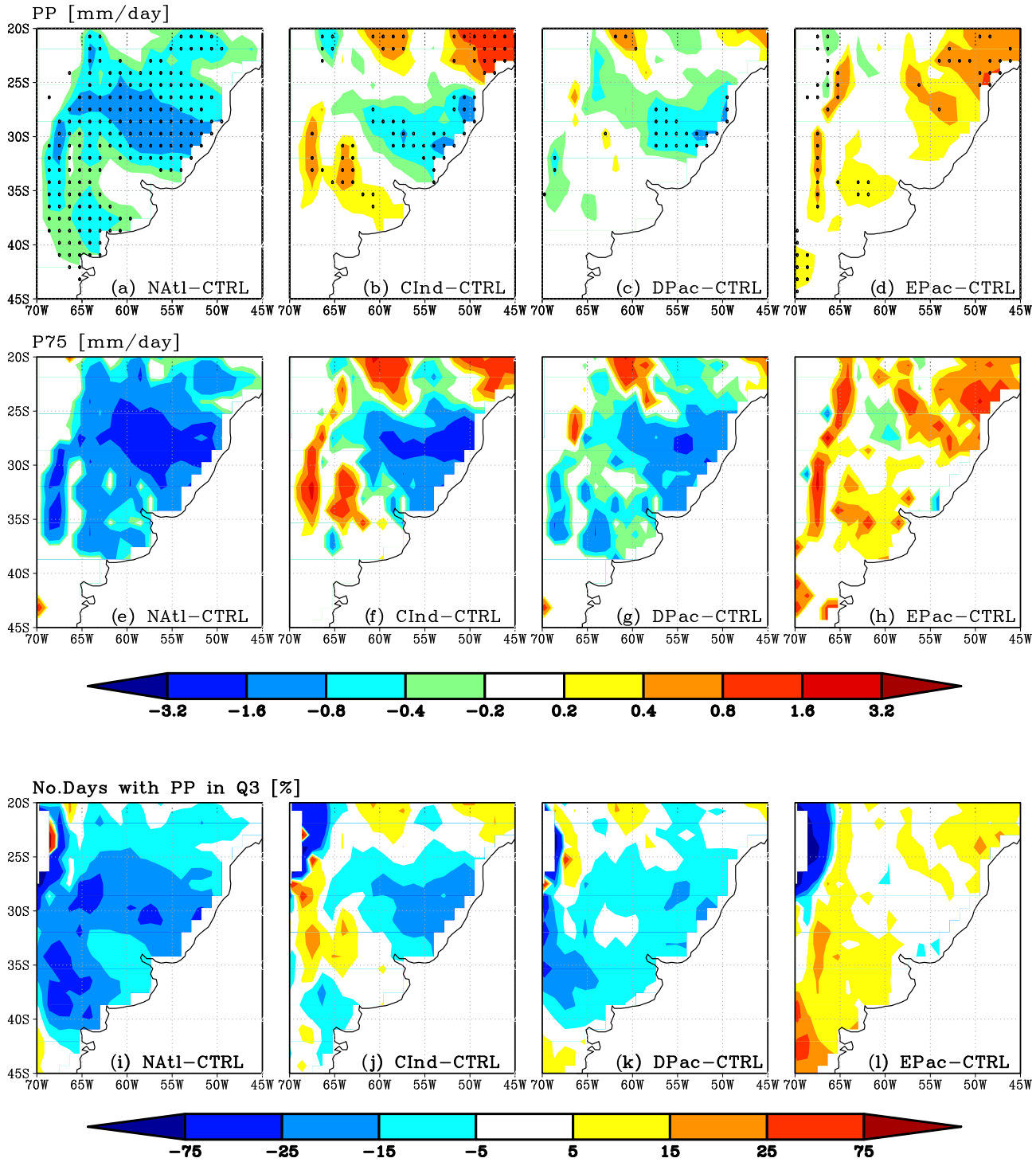

Fig. 8. (First row) Precipitation anomalies (sensitivity experiment minus CTRL): (a) North Atlantic, (b) Central Indian, (c) Pacific Dateline and (d) East Pacific experiment. The significance was tested through a Student's *t*-test. Dots indicate where the differences are statistical significant at 95%. (Second row) As first row but for the threshold of the percentile 75. Panels displaying differences refers to the same color bar, units are mm/day and values lower than |0.2| are obscured. (Third row) Number of days in sensitivity experiments with precipitation exceeding the threshold of the percentile 75 of the CTRL run. Units are %, and values lower than |5| are obscured. All panels are for October–November.

eastern sector of the domain (around the southern tip of Brazil), which is also characterized by a high coupling between soil moisture and evapotranspiration, is less affected by differences in circulation. Therefore differences in the precipitation indices in this area are partly explained by land–atmosphere feedbacks.

The hot-spot area with maximum soil moisture-precipitation coupling is located around the boundary between Argentina and Uruguay (Sörensson and Menéndez, 2011). The fact that in this area the differences between both ensembles (W–S) are relatively small suggests that competing feedbacks can be associated with local soil moisture effects and regional scale circulation. Complementary analysis to identify the reasons for the geographical pattern of the differences between both ensembles in these and other relevant indices is ongoing.

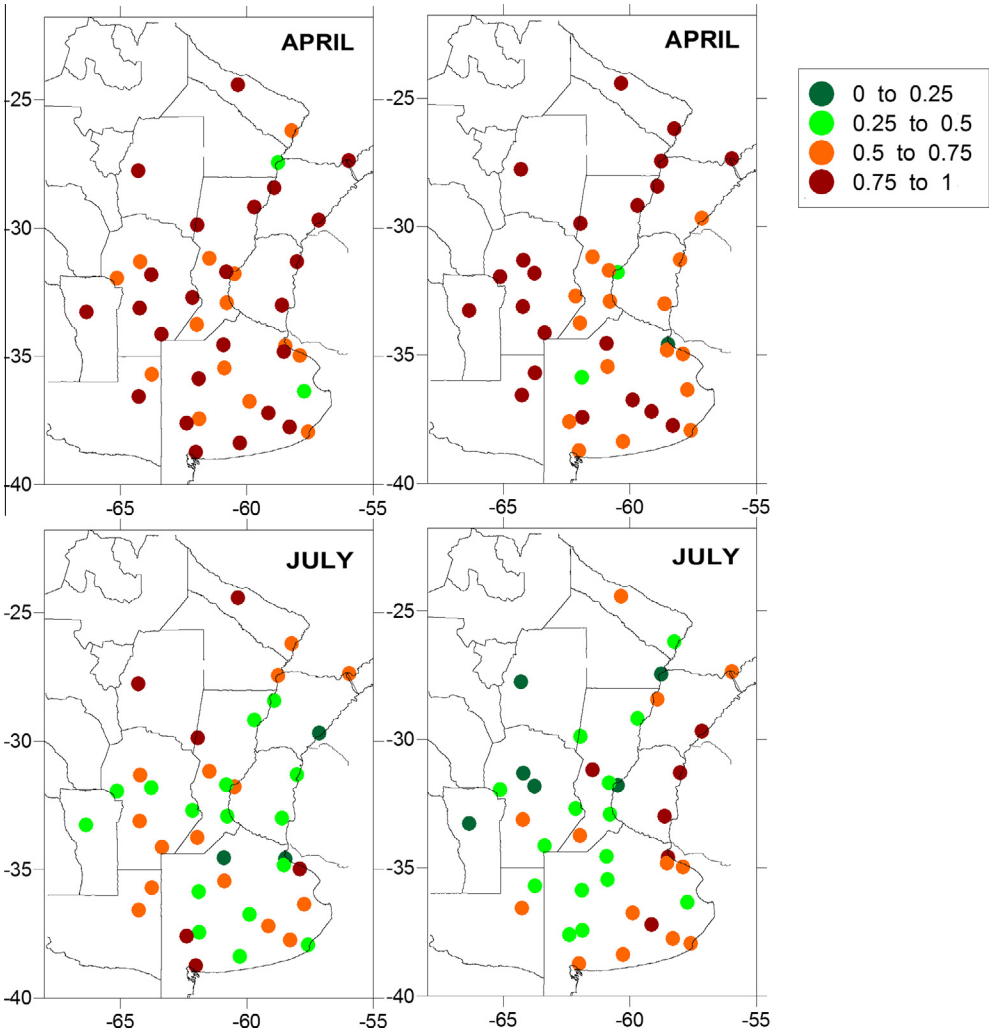

Fig. 9. Percentage of extreme unfavorable hydric condition that coincides with extreme high potential evapotranspiration (left) or extreme low rainfall (right), for the period 1970–2010.

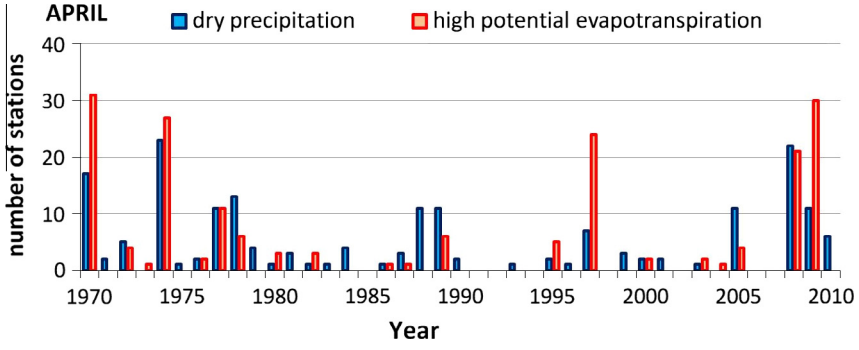

Fig. 10. Number of stations under extreme high potential evapotranspiration (red bar) and extreme dry precipitation (blue bar) for April, period 1970–2010. (For interpretation of the references to color in this figure legend, the reader is referred to the web version of this article.)

5. Indices of precipitation extremes over LPB

Indices are useful to compare the wet and dry aspects (frequency, intensity) and their trends in several areas. In this section, daily and monthly indices are calculated for the LPB region, discussing the occurrence of droughts, dry spells, daily wet extremes, comparing observations and model simulations, and analyzing projections for the future climate.

5.1. SPI index – Droughts in LPB-observations

Droughts are a recurrent phenomenon over LPB, with impacts evident in the reduction of crop yields, reduced cattle products, streamflow deficiencies, and consequent problems for hydroelectric power generation. Therefore, the quantitative knowledge of the properties of droughts in LPB is an important aspect of the planning and management of agricultural practices and water resources.

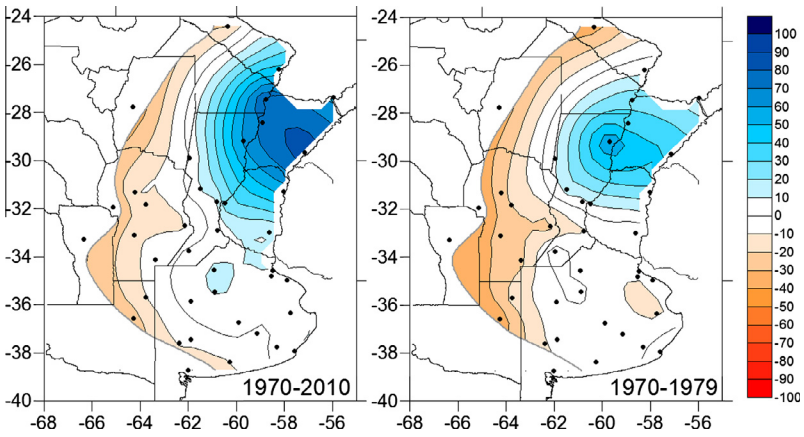

Fig. 11. Hydric condition (mm) for April in two different periods: 1970–79 (right) and 1970–2010 (left). Dots show location of stations.

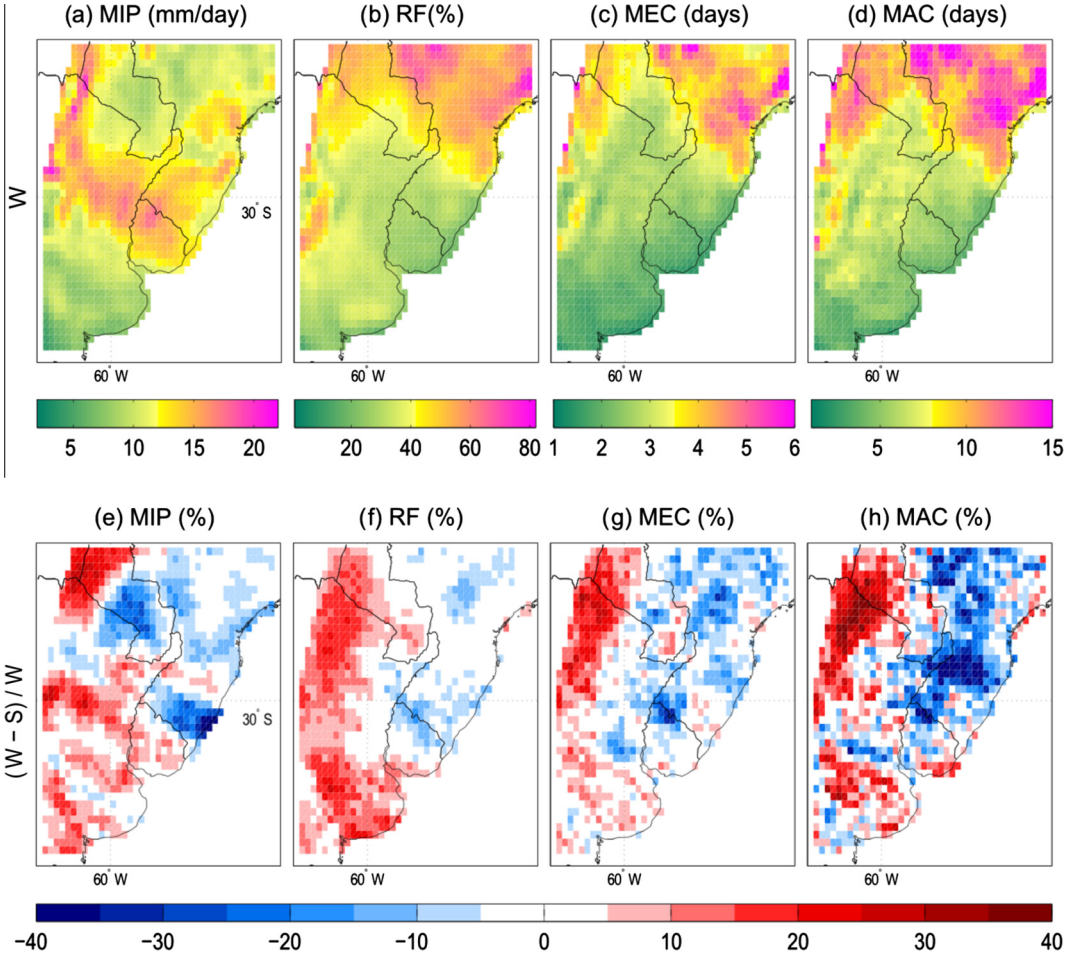

Fig. 12. Upper panels (a–d) show the precipitation indices of ensemble W. (a) mean daily intensity of precipitation (MIP), (b) relative frequency of wet days (RF), (c) mean length of consecutive wet days (MEC) and (d) maximum length of consecutive wet days (MAC). Lower panels (e–h) show the differences in the same indices between the ensembles (W–S), expressed as a percentage of the values of W.

The SPI is one of the drought indices most widely used worldwide, and one of the best suited for the area of study (Rivera and Penalba, 2011). The SPI index (see Section 2.3) is computed on time scales of 12 months (SPI12) to show the main features of the long-term droughts. A drought event is considered as the period of time when SPI values are below −1.0, which means that the precipitation departures from average conditions exceed one standard deviation.

Fig. 13 shows the number of drought events, together with the mean duration and severity of those events for the period 1962–2008 in the CLARIS-LPB dataset (Penalba et al., 2014). The region that records the highest number of drought events (more than 20) corresponds to those with the shorter durations of dry conditions (between 3 and 5 months) and is located over the central-eastern portion of Argentina and Paraguay (Fig. 13a and b). The spatial distribution of the SPI index (Fig. 13c) shows that the

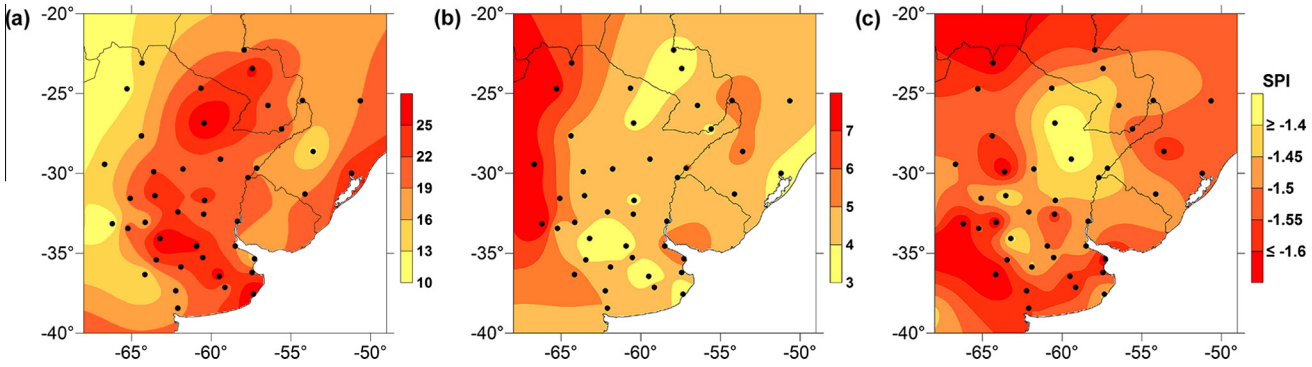

Fig. 13. Drought characteristics in La Plata Basin: (a) number of events; (b) mean duration (months) and (c) severity (SPI index). Period 1962–2008. Dots show location of stations.

central-western portion of Argentina is more prone to record severe droughts (SPI12 $\leqslant -1.5$), while most of the LPB records show, on average, moderate drought conditions.

The DHI (Fig. 14) shows that most of the regions with moderate to high drought hazard are located in the western and southern portions of LPB, while low drought hazard occurs in northeastern Argentina, southern Brazil, and Paraguay. The increases in precipitation during the second half of the 20th century, in the western portion of the region, led to an expansion of the agricultural frontier (Barros et al., 2008). In these regions it is necessary to carry out contingency and mitigation plans in order to reduce the impacts of droughts. This map, along with a vulnerability map of the region, will allow the construction of a droughts risk map.

5.2. Indices of dry spells in LPB in future climate

Dry spells in LPB are analyzed following the methodology of Sánchez et al. (2011). A precipitation threshold of less than 1.0 mm/day is used to define a dry day. The indices, related to the extremes in the left tail of the statistical distribution of the daily precipitation, are the maximum length of dry spells (Max-DSL), its mean length (Mean-DSL), the total number of days without precipitation (Nb-noPPd) and the total number of dry spell events (Nb-DS).

The impact of climate change on dry spells indices obtained from regional models described in Section 2.2 is shown in Table 1 which presents the four DS related indices: (Max-DSL), (Mean-DSL), (Nb-noPPd) and (Nb-DS). The indices are calculated in every grid point, but values in the table correspond to the mean index in a certain box: La Plata Basin (LPB, 14°S–37°S, 43°W–67°W), the Brazilian Plateau (BP, 0°S–15°S, 35°W–50°W), Pampa, Central and North Argentina (PCNA, 20°S–40°S, 55°W–70°W) and Central Patagonia (CP, 43°S–50°S, 65°W–73°W).

Relative DS length changes are lower than 13% for all regions. Regions with high sensitivity are characterized by similar rates of change in both Max-DSL and Mean-DSL (e.g. BP and CP). On the other hand, there are some regions with a rate of change of about 6–10% in the maximum DSL but with small changes (or with a decreasing rate) in the mean DSL (e.g. LPB and PCNA). The probability distribution of the DSL in a warmer climate is box dependent. However, a common feature to the four considered areas is that there is greater variability in the length of dry spells in the future climate, which is primarily associated with a shift to the right in the DSL distribution of the Max-DSL index (the Mean-DSL index has minor changes). So, in a warmer climate the probability distribution function of the DSL is expected to be flatter than in the present climate (not shown).

Regarding the number of no-precipitation days (Nb-noPPd index) and the number of DS (Nb-DS index), their rates of change for a warmer climate are smaller than the corresponding rates of change of the previous indices. The major changes are in the BP region, where models project a smaller number of DS, but with longer duration events. A note of caution that must be taken into account concerning these indices is that changes (future minus present) are much smaller than the inter-model spread (i.e., the signal to noise rate is low).

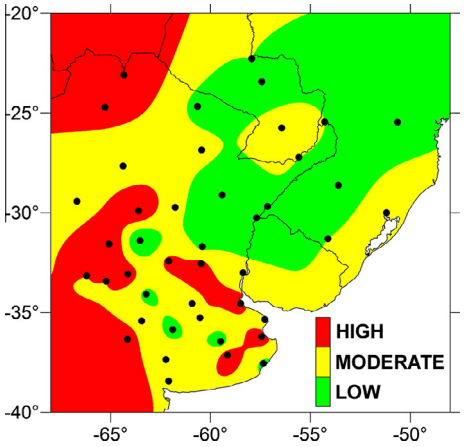

Fig. 14. Drought hazard map for the period 1962–2008. Dots show location of stations.

5.3. DIER – Index of daily wet extremes intensity in LPB-observations

Daily precipitation from the CLARIS-LPB dataset is used to analyze the intensity of daily extreme rainfall (DIER index). The relation between climate indices and extreme precipitation over LPB is analyzed through correlations of reconstruction of the dominant periods of precipitation variability from Multitaper spectrum periods and Pacific Decadal Oscillation (PDO), Atlantic multidecadal oscillation (AMO), Tropical South Atlantic (TSA), Indian Dipole Ocean (IOD) and El Niño 3.4.

Extreme events are infrequent meteorological phenomena that surpass a defined threshold and depend strongly on location. Fig. 15 presents the seasonal mean value of the 75th daily percentile (P75) for the period 1992–2000 of each season. Over Southeastern Brazil the values decrease from summer to winter, consistent with the annual cycle of precipitation. Similar values during the four seasons over southern Brazil are also consistent with the uniform precipitation during the year.

Table 1
Dry spell indices. First column indicates the four regions in which indices are presented: La Plata Basin (LPB), Brazilian Plateau (BP), Pampa-Central-North Argentina (PCNA) and Central Patagonia (CP). Second column displays the index: Maximum dry spell length (DSL), mean dry spell length, the number of days without precipitation (Nb-noPPd) and the number of dry spell events (Nb-DS). All indices are expressed in days. Third and fourth columns are indexes for the ensemble mean (ENS), present and future climate respectively; fifth column shows the rate of change [%] when the climate warms.

	Indices	ENS present climate 1969–1990 [days]	ENS future climate 2070–2100 [days]	Rate of change [%]
LPB region	Max DSL	103.3	113.4	9.8
	Mean DSL	10.4	10.5	0.9
	Nb-noPPd	7759.9	7782.8	0.3
	Nb-DS	524.3	523.8	−0.1
BP region	Max DSL	139.2	156.3	12.4
	Mean DSL	13.1	14.8	13.3
	Nb-noPPd	5962.9	6423.5	7.7
	Nb-DS	323.4	312.0	−3.6
PCNA region	Max DSL	137.3	145.3	5.8
	Mean DSL	14.7	14.2	−2.9
	Nb-noPPd	8914.4	8761.0	−1.7
	Nb-DS	477.4	489.8	2.6
CP region	Max DSL	67.1	73.9	10.2
	Mean DSL	8.7	9.7	11.6
	Nb-noPPd	7762.2	7857.4	1.2
	Nb-DS	614.4	605.5	−1.5

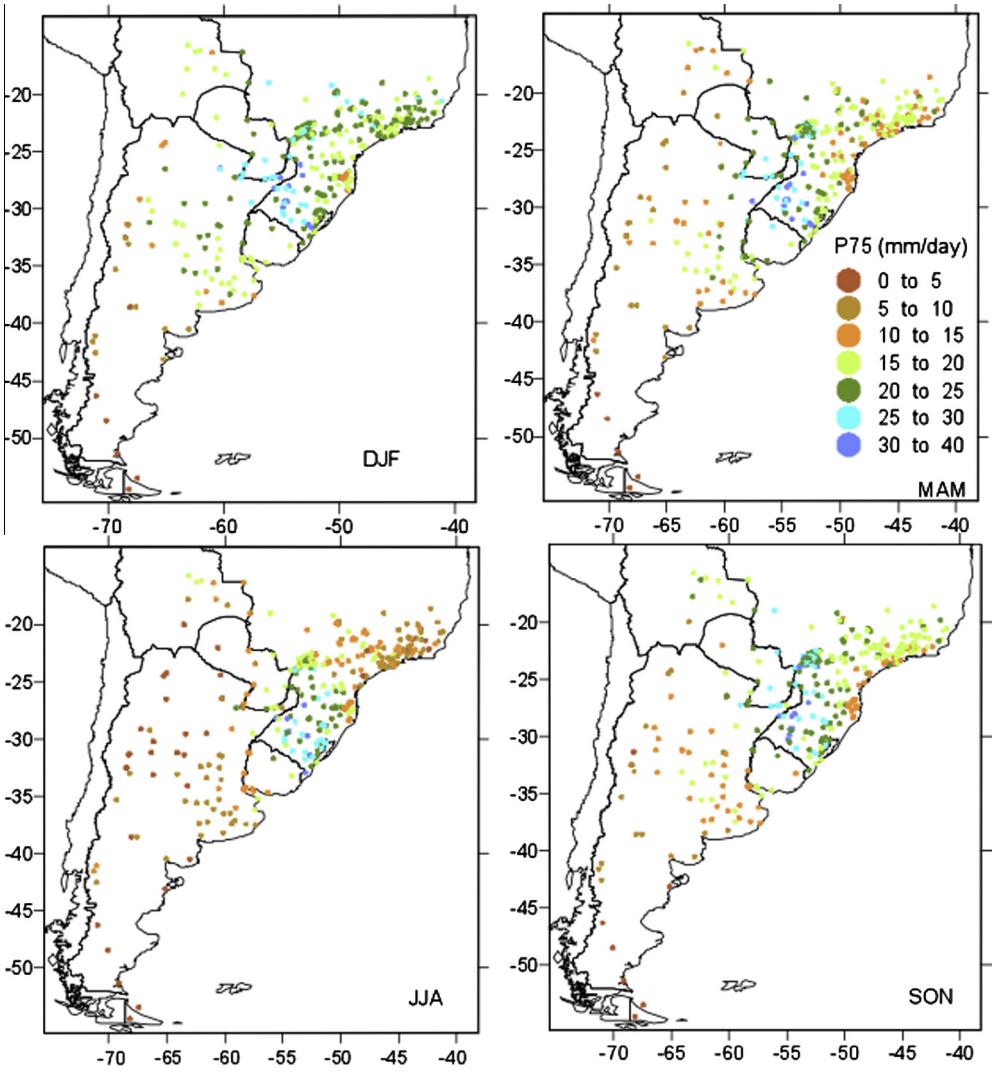

Fig. 15. Seasonal mean value of DIER75 for the period 1992–2000. Dots show location of stations.

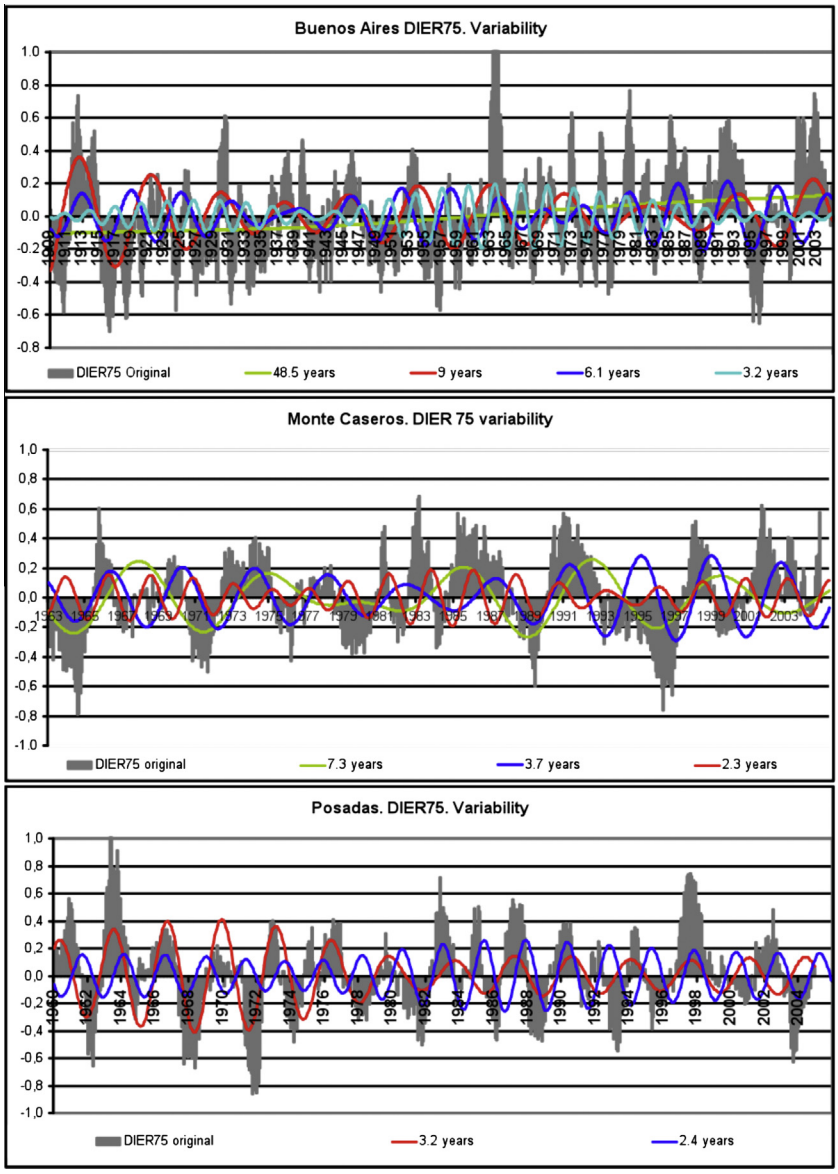

Fig. 16. Reconstruction of the dominant periods of variability from Multitaper spectrum periods, significant at 95%. Top: Buenos Aires (34°36′S 58°22′W), period of analysis 1908–2005. Middle: Monte Caseros (30°15′S 57°38′W), 1963–2005, bottom: Posadas (27°21′S 55°53′W), 1960–2005.

In Argentina there are different extreme values between summer and winter. Fig. 16 shows the dominant period of variability for DIER75 at Buenos Aires, Monte Caseros, and Posadas stations. The extreme rainfall can be explained by the combination of different periodicities, for example in Buenos Aires, extreme rainfall in 1964 presents a conjugation of 3.2, 6.1 and 9 years periods. Monte Caseros presents periods of variability of 7.3, 3.7 and 2.3 years. Posadas shows significant variability at 3.2 and 2.4 years. Table 2 shows the correlation between sea climate indices and the variability in the three locations. The highest correlations are found in Buenos Aires for Pacific Decadal Oscillation (PDO) and Tropical South Atlantic (TSA). El Nino SST index, although with lower correlation, has also significant values. Relations between South America rainfall and PDO have been analyzed by Kayano and Andreoli (2007), where they indicated that the differences in the strength of ENSO teleconnections for the South American rainfall might be related to the PDO, which creates a background for these teleconnections acting constructively (destructively) when ENSO and PDO are in the same (opposite) phase. In the present paper we present only the

Table 2
Correlation between sea climate indices and reconstruction of the dominant mode. Top: Buenos Aires (34°36′S 58°22′W) period of analysis 1908–2005. Middle: Monte Caseros (30°15′S 57°38′W) 1963–2005, bottom: Posadas (27°21′S 55°53′W). Significant values are shown in bold. Pacific Decadal Oscillation (PDO), Atlantic multidecadal oscillation (AMO), Tropical South Atlantic (TSA), Indian Dipole Ocean (IOD) and El Niño 3.4.

Buenos Aires	PDO	AMO	TSA	IOD	NIño3.4
Original	**0.18**	−0.07	**0.17**	0.07	**0.23**
Non linear trend	**0.43**	**−0.14**	**0.43**	0.01	**0.11**
9 years	−0.05	−0.03	0.07	0.06	0.02
6.1 years	**0.17**	0.03	0.01	**−0.20**	**0.18**
3.2 years	0.07	0.03	0.09	0.05	**0.12**
Mte Caseros	PDO	AMO	TSA	IOD	NIño3.4
Original	**0.17**	0.05	0.05	0.17	0.30
7.2 years	−0.01	**−0.15**	−0.03	−0.02	−0.02
3.7 years	0.03	**0.14**	**0.14**	**0.22**	**0.27**
2.3 years	**0.17**	−0.01	−0.09	**0.17**	**0.21**
Posadas	PDO	AMO	TSA	IOD	NIño3.4
Original	**0.17**	**0.11**	0.08	**0.18**	**0.37**
3.2 years	**0.16**	**0.18**	**0.13**	**0.18**	**0.26**
2.4 years	−0.04	−0.03	−0.03	0.05	**0.25**

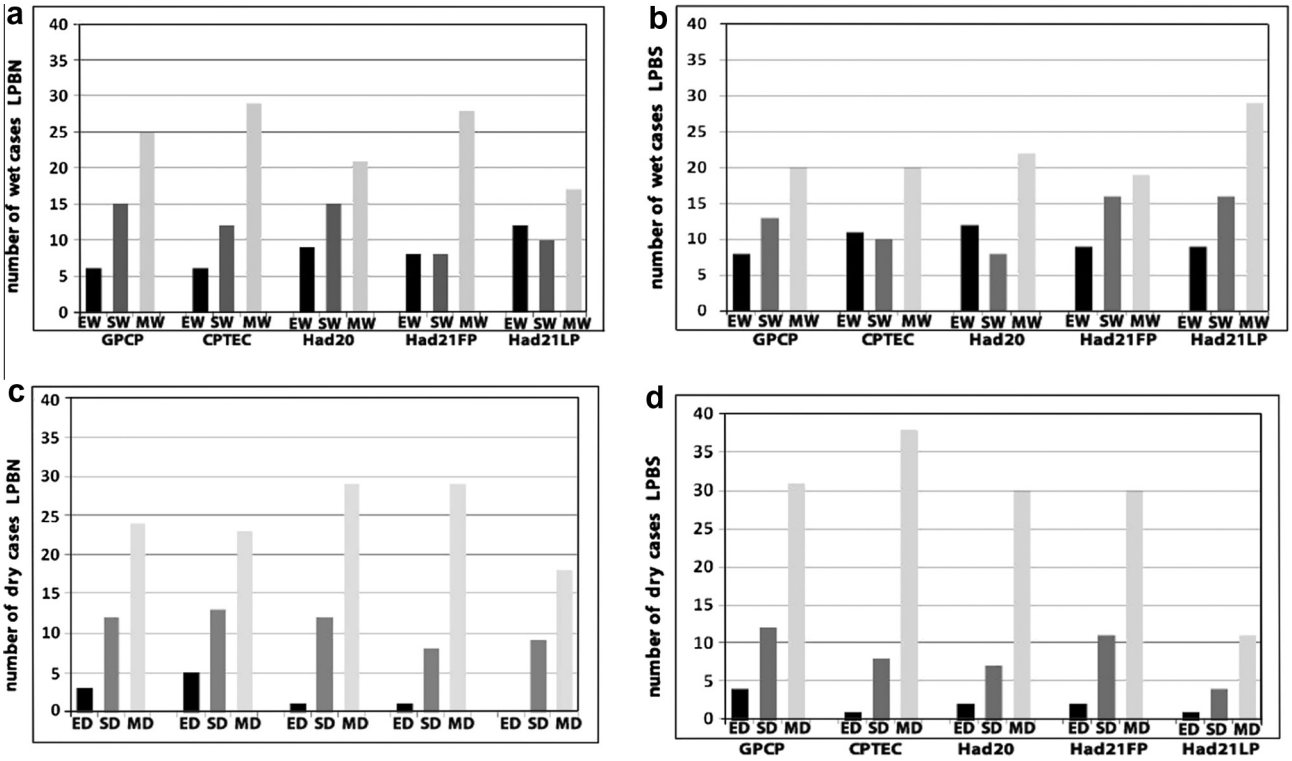

Fig. 17. Number of cases in each category (E: extreme, S: severe, M: moderate) and each sector of LPB for GPCP and CPTEC/INPE AGCM, HadCM3 (Had20) simulations in the 20th century and projections of HadCM3 (first period of 21st century: Had21FP and last period of 21st century: Had21LP). (a) wet in the north, (b) wet in the south, (c) dry in the north, (d) dry in the south.

statistical relationships between rainfall and PDO, and the dynamic features are been analyzed in other studies.

5.4. SPI index – Frequency of monthly wet and dry extremes over two sectors of La Plata Basin-observations and Model results

The frequency of precipitation extremes using SPI is analyzed in two sectors of La Plata Basin: northern (15°S–25°S; 55°W–45°W) and southern (25°S–35°S; 60°W–50°W) using observed data and two global models in order to verify the models performance and the future projections. Monthly data during 1979–2001 are taken from GPCP precipitation and from CPTEC/INPE AGCM. Simulations and projections from HadCM3 are analyzed during 3 periods (1979–1999, 2000–2020, 2079–2099).

The frequency of extreme, severe, and moderate precipitation events (wet and dry) in the northern (NLPB) and southern (SLPB) sectors based on the Standardized Precipitation Index (SPI) are shown in Fig. 17 for each dataset, model and period. The frequency of observed monthly wet extremes is higher than the frequency of dry extremes in both sectors. The frequency of wet cases is higher in SLPB than in NLPB. Both models reproduce these features. Moreover, both models overestimate the frequency of extreme wet cases and underestimate the number of extreme dry cases in the southern sector. In the northern sector, the frequency of wet extremes in CPTEC results is similar to GPCP, and HadCM3 presents more wet cases than observed.

Comparing the HadCM3 frequency simulated in the present time with the projections, the behaviors of the three categories of extremes are different in the two LPB sectors. In the near future (2000–2020), the frequency of extreme wet cases decreases in the northern and southern sectors, but the number of moderate (severe) cases increases in the northern (southern) sector (Fig. 17a and b). The projections for the last period of the 21st century (2079–2099) indicate an increase of extreme wet cases in the northern sector and an increase of severe and moderate wet cases in the southern sector, compared with the 20th century. The number of moderate dry extremes reduces in the northern sector and increases in the southern sector in the near future (Fig. 17c and d). The frequencies of extreme and moderate dry cases are similar in the 20th century and near future, but the extreme and severe dry cases reduces in the last period of 21st century in both sectors.

6. Conclusion

The La Plata Basin is a region highly populated with one of the largest hydroelectric power plant in the world, agriculture areas and industries. The region is affected by droughts and floods, which cause severe damages to the social life and economy. Therefore, the study of precipitation extremes (wet and dry conditions) is a relevant theme and indicators for the extremes can be applied in plans of vulnerability and adaptation strategies. Large-scale influences on extremes over LPB from observations and global models results are found from the Pacific, Indian and Atlantic Oceans. January wet precipitation extremes obtained from monthly SPI are mostly affected by a wavetrain from the western Pacific in the northern sector of LPB while the wet extremes in the southern sector are mostly influenced by a wavetrain from the Indian Ocean. These wavetrains affect the northern and southern sectors in opposite ways, resulting in a precipitation dipole, but the sources of the teleconnections are located in different oceans. More specifically, idealized model experiments show that warm anomalies in the North Atlantic, Central Pacific and Central Indian Oceans induce reductions of daily precipitation extremes in large areas of LPB. On the other hand, a warm SST anomalous forcing in the Eastern Pacific implies increased daily precipitation extremes, mainly in the northern sector of LPB.

The frequency of extremes is also related to ENSO episodes and it can be modulated by the different types of ENSO defined in the

literature (i.e. Kug et al., 2009; Ashok et al., 2007). In fact, in Canonical El Niño (La Niña) years the frequency of extremes is higher (lower) than in neutral years. However in specific cases (i.e. ENSO Modoki + A), the northern sector of the LPB displays increased (reduced) number of extremes during La Niña (El Niño) events, and the southern sector shows an opposite pattern.

In terms of local processes and feedbacks between soil moisture, evapotranspiration and precipitation, it is shown that April is the most risky month for crop production due to the relation between precipitation and evapotranspiration. It is demonstrated that the soil moisture affects precipitation indices. In fact the comparison between experiments with and without soil moisture–atmosphere interaction evidenced a west-east pattern that indicated more intense and frequent extremes, as well as longer wet periods over Paraguay and Argentina when soil moisture atmosphere interaction is activated and the opposite over southern and central-southern Brazil. This result indicates that knowledge of soil moisture could help in the prediction of summer precipitation extreme events.

The statistics of observed dry and wet conditions show that the highest frequency of droughts during 1962–2008 occurred in central–eastern Argentina and Paraguay. There are differences in the frequency of monthly wet and dry extremes in the northern and southern sectors of LPB. The CPTEC/INPE AGCM and HadCM3 reproduce these differences. Indices of dry spells in future projections show small changes compared to present climate, but the probability distribution function of maximum length will shift to the right, indicating longer duration of the events.

Other studies using the regional models from CLARIS-LPB are in development to assess other aspects of climate change related to extremes over La Plata Basin.

Acknowledgements

The research leading to these results received funding from the European Community's Seventh Framework Programme FP7/2007–2013) under Grant Agreement N° 212492: CLARIS LPB. A Europe–South America Network for Climate Change Assessment and Impact Studies in La Plata Basin. The first author is also grateful to CNPq and FAPESP for the research support.

References

Adler, R.F., Huffman, G.J., Chang, A., Ferraro, R., Xie, P., Janowiak, J., Rudolf, B., Schneider, U., Curtis, S., Bolvin, D., Gruber, A., Susskind, J., Arkin, P., Nelkin, E., 2003. The version 2 global precipitation climatology project (GPCP) monthly precipitation analysis (1979–present). J. Hydrometeor. 4, 1147–1167.

Ashok, K., Behera, S.K., Rao, S.A., Weng, H., Yamagata, T., 2007. El Niño Modoki and its possible teleconnection. J. Geophys. Res. 112, C11007.

Ashok, K., Yamagata, T., 2009. Climate change: El Nino with a difference. Nature 461, 481–484.

Barros, V., Gonzalez, M., Liebmann, B., Camilloni, I.A., 2000. Influence of the South Atlantic convergence zone and South Atlantic sea surface temperature on interannual summer rainfall variability in southeastern South America. Theor. Appl. Climatol. 67, 123–133.

Barros, V.R., Doyle, M.E., Camilloni, I.A., 2008. Precipitation trends in southeastern South America: relationship with ENSO phases and with low-level circulation. Theor. Appl. Climatol. 93, 19–33.

Barros, V.R., Garavaglia, C.R., Doyle, M.E., 2013. Twenty-first century projections of extreme precipitations in the Plata Basin. Int. J. River Basin Manage. 11, 373–387.

Berbery, E.H., Collini, E.A., 2000. Springtime precipitation and water vapor flux over southeastern South America. Mon. Wea. Rev. 128, 1328–1346.

Berbery, E.H., Barros, V.R., 2002. The hydrologic cycle of the La Plata Basin in South America. J. Hydrometeor. 3, 630–645.

Berbery, E.H., Doyle, M., Barros, V.R., 2006. Tendencias regionales en la precipitacion. In: Barros, V., Clarke, R., Silva Dias., P. (Eds.), El Cambio climático en la cuenca del Plata. Buenos Aires, CIMA/CONICET, pp. 67–79.

Berri, G.J., Bertossa, G.I., 2004. The influence of the tropical and subtropical Atlantic and Pacific Oceans on precipitation variability over Southern Central South America on seasonal time scales. Int. J. Climatol. 24, 415–435.

Boulanger, J.P., Leloup, J., Penalba, O.C., Rusticucci, M.M., Lafon, F., Vargas, W.M., 2005. Observed precipitation in the Paraná-Plata hydrological basin: long-term trends, extreme conditions and ENSO teleconnections. Clim. Dyn. 24, 393–413.

Boulanger, J.P., Brasseur, G., Carril, A.F., Castro, M., Degallier, N., Ereño, C., Marengo, J.A., Le Treut, H., Menéndez, C., Nuñez, M., Penalba, O., Rolla, A., Rusticucci, M., Terra, R., 2010. The European CLARIS project: a Europe–South America network for climate change assessment and impact studies. Clim. Change 98, 307–329.

Camargo, A.P., Marin, F.R., Sentelhas, P.C., Giarola, P.A., 1999. Ajuste de equação de Thornthwaite para estimar la evapotranspiração em climas arido y superhumedo, com base na amplitude térmica diária. Rev. Bras. Agrometeorologia 7, 251–257.

Camilloni, I.A., Barros, V.R., 2003. Extreme discharge events in the Paraná River and their climate forcing. J. Hydrol. 278, 94–106.

Carril, A.F., Menéndez, C.G., Remedio, A.R.C., Robledo, F., Sörensson, A., Tencer, B., Boulanger, J.P., Castro, M., Jacob, D., Le Treut, H., Li, L.Z.X., Penalba, O., Pfeifer, S., Rusticucci, M., Salio, P., Samuelsson, P., Sanchez, E., Zaninelli, P., 2012. Performance of a multi-RCM ensemble for South Eastern South America. Clim. Dyn. 39, 2747–2768.

Carvalho, L.M.V., Jones, C., Liebmann, B., 2002. Extreme precipitation events in southeastern South America and large-scale convective patterns in the South Atlantic convergence zone. J. Clim. 15, 2377–2394.

Carvalho, L.M.V., Jones, C., Liebmann, B., 2004. The South Atlantic convergence zone: intensity, form, persistence, relationships with intraseasonal to interannual activity and extreme rainfall. J. Clim. 17, 88–108.

Cavalcanti, I.F.A., Kayano, M.T., 1999. High-frequency patterns of the atmospheric circulation over southern hemisphere and South America. Meteorol. Atmos. Phys. 69, 179–193.

Cavalcanti, I.F.A., Marengo, J.A., Satyamurty, P., Nobre, C.A., Trosnikov, I., Bonatti, J.P., Manzi, A.O., Tarasova, T., Pezzi, L.P., D'Almeida, C., Sampaio, G., Castro, C.C., Sanches, M.B., Camargo, H., 2002. Global climatological features in a simulation using CPTEC/COLA AGCM. J. Clim. 15, 2965–2988.

Cavalcanti, I.F.A., Camilloni, I., Ambrizzi, T., 2006. Escenarios climaticos regionales. In: Barros, V., Clarke, R., Silva Dias, P. (Eds.). El Cambio climático en la cuenca del Plata. Buenos Aires, CIMA/CONICET, pp. 175–190.

Cavalcanti, I.F.A., Shimizu, M.H., 2012. Climate fields over South America and variability of SACZ and PSA in HadGEM-ES. Am. J. Clim. Change 1, 132–144.

Cavalcanti, I.F.A., 2012. Large scale and synoptic features associated with extreme precipitation over South America: a review and case studies for the first decade of the 21st century. Atmos. Res. 118, 27–40.

Chamorro, L., 2006. Los principales usos y problemas de los recursos hídricos. In: Barros, V., Clarke, R., Silva Dias, P. (Eds.), El Cambio climático en la cuenca del Plata. Buenos Aires, CIMA/CONICET, pp. 111–123.

Chan, S., Behera, S., Yamagata, T., 2008. Indian Ocean dipole influence on South American rainfall. Geophys. Res. Lett., 35 L14S12

Cherchi, A., Carril, A., Menendez, C., Zamboni, L., 2014. La Plata Basin precipitation variability in spring: role of remote SST forcing as simulated by GCM experiments. Clim. Dyn. 42, 219–236.

Chou, S.C., Marengo, J.A., Lyra, A., Sueiro, G., Pesquero, J., Alves, L.M., Kay, G., Betts, R., Chagas, D., Gomes, J.L., Bustamante, J., Tavares, P., 2012. Downscaling of South America present climate driven by 4-member HadCM3 runs. Clim. Dyn. 38, 635–653.

Cunningham, C.C., Cavalcanti, I.F.A., 2006. Intraseasonal modes of variability affecting the South Atlantic Convergence Zone. Int. J. Climatol. 26, 1165–1180.

da Rocha, R.P., Rodrigues, C.A.M., Cuadra, S.V., Ambrizzi, T., 2009. Precipitation diurnal cycle and summer climatology assessment over South America: an evaluation of regional climate model version 3 simulations. J. Geophys. Res. 114, 1–19.

Diaz, A.F., Studzinski, C.D., Mechoso, C.R., 1998. Relationships between precipitation anomalies in Uruguay and southern Brazil and sea surface temperature in the Pacific and Atlantic Oceans. J. Clim. 11, 251–271.

Doyle, M.E., Barros, V.R., 2002. Midsummer low-level circulation and precipitation in subtropical South America and related sea surface temperature anomalies in the South Atlantic, 2002. J. Clim. 15, 3394–3410.

Forte Lay, J.A., Spescha, L., 2001. Método para la estimación de la climatología del agua edáfica en las provincias pampeanas de la Argentina. Rev. Argentina Agrometeorologia 1, 67–74.

Giorgi, F., Jones, C., Asrar, G.R., 2009. Addressing climate information needs at the regional level: the CORDEX framework. World Meteorological Organization (WMO). Bulletin 58 (3), 175.

Gordon, C., Cooper, C., Senior, C.A., Banks, H.T., Gregory, J.M., Johns, T.C., Mitchell, J.F.B., Wood, R.A., 2000. The simulation of SST, sea ice extents and ocean heat transports in a version of the Hadley Centre coupled model without flux adjustments. Clim. Dyn. 16, 147–168.

Grimm, A.M., Ferraz, S.E.T., Gomes, J., 1998. Precipitation anomalies in southern Brazil associated with El Nino and La Nina events. J. Climate 11, 2863–2880.

Grimm, A.M., Barros, V.R., Doyle, M.E., 2000. Climate variability in southern South America associated with El Nino and La Nina events. J. Clim. 13, 35–58.

Grimm, A.M., 2003. The El Niño impact on summer monsoon in Brazil: regional processes versus remote influences. J. Clim. 16, 263–280.

Grimm, A.M., 2004. How do La Niña events disturb the summer monsoon system in Brazil? Clim. Dyn. 22, 123–138.

Grimm, A.M., Natori, E.A.A., 2006. Climate change and interannual variability of precipitation in South America. Geophys. Res. Lett. 33, L19706, 10.1029/2006GL026821.

Grimm, A.M., Tedeschi, R.G., 2009. ENSO and extreme rainfall events in South America. J. Clim. 22, 1589–1609.

Grimm, A.M., 2011. Interannual climate variability in South America: impacts on seasonal precipitation, extreme events and possible effects of climate change. Stoch. Env. Res. Risk Assess. 25, 537–554.
Hayes, M.J., Svoboda, M.D., Wilhite, D.A., Vanyarkho, O.V., 1999. Monitoring the 1996 drought using the standardized precipitation index. Bull. Amer. Meteor. Soc. 80, 429–438.
Heim, R.R., 2002. A review of twentieth-century drought indices used in the United States. Bull. Am. Meteor. Soc. 83, 1149–1165.
Hourdin, F., Musat, I., Bony, S., Braconnot, P., Codron, F., Dufresne, J.L., Fairhead, L., Filiberti, M.A., Friedlingstein, P., Grandpeix, J.X., Krinner, G., LeVan, P., Li, Z.X., Lott, F., 2006. The LMDZ4 general circulation model: climate performance and sensitivity to parametrized physics with emphasis on tropical convection. Clim. Dyn. 27, 787–813.
Jacob, D., Elizalde, A., Haensler, A., Hagemann, S., Kumar, P., Podzun, R., Rechid, D., Remedio, A.R., Saeed, F., Sieck, K., Teichmann, C., Wilhelm, C., 2012. Assessing the transferability of the regional climate model REMO to Different COordinated Regional Climate Downscaling EXperiment (CORDEX) regions. Atmosphere 3, 181–199.
Jones, C., Carvalho, L.M.V., 2013. Climate change in the South American monsoon system: present climate and CMIP5 projections. J. Clim. 26, 6660–6678.
Junquas, C., Vera, C., Li, L., Le Treut, H., 2012. Summer precipitation variability over southeastern South America in a global warming scenario. Clim. Dyn. 38, 1867–1883.
Kayano, M.T., Andreoli, R.V., 2007. Relations of South American summer rainfall interanual variations with the Pacific Decadal Oscillation. Int. J. Climatol. 27, 531–540.
Kjellström, E., Boberg, F., Castro, M., Christensen, J.H., Nikulin, G., Sánchez, E., 2010. Daily and monthly temperature and precipitation statistics as performance indicators for regional climate models. Clim. Res. 44, 135–150.
Kodama, Y., 1992. Large scale common features of subtropical precipitation zones (the Baiu Frontal Zone, the SPCZ, and the SACZ). Part I: Characteristics of subtropical frontal zones. J. Meteorol. Soc. Jpn 70, 813–836.
Kousky, V.E., Kagano, M.T., Cavalcanti, I.F.A., 1984. A review of the Southern Oscillation: Oceanic–atmospheric circulation changes and related rainfall anomalies. Tellus 36A, 490–504.
Koster, R.D., Guo, Z., Dirmeyer, P.A., Bonan, G., Chan, E., Cox, P., Davies, H., Gordon, C.T., Kanae, S., Kowalczyk, E., Lawrenc, D., Liu, P., Lu, C.H., Malyshev, S., McAvaney, B., Mitchell, K., Mocko, D., Oki, T., Oleson, K.W., Pitman, A., Sud, Y.C., Taylor, C.M., Verseghy, D., Vasic, R., Xue, Y., Yamada, T., 2006. GLACE: the global land-atmosphere coupling experiment: Part I: Overview. J. Hydrom. 7, 590–610.
Kug, J.S., Jin, F.F., An, S.-I., 2009. Two types El Niño events: cold tongue El Niño and warm pool El Niño. J. Clim. 22, 1499–1515.
Liebmann, B., Kiladis, G.N., Marengo, J.A., Ambrizzi, T., Glick, J.D., 1999. Submonthly convective variability over South America and the South Atlantic convergence zone. J. Clim. 12, 1877–1891.
Liebmann, B., Jones, C., Carvalho, L.M.V., 2001. Interannual variability of extreme precipitation events in the state of São Paulo, Brazil. J. Clim. 14, 208–218.
Liebmann, B., Vera, C.S., Carvalho, L.M.V., Camilloni, I.A., Hoerling, M.P., Allured, D., Barros, V.R., Báez, J., Bidegain, M., 2004. An observed trend in central South American precipitation. J. Clim. 17, 4357–4367.
McKee, B., Doesken, N.J., Kleist, J., 1993. The Relationship of drought frequency and duration to time scales, 1993. In: Proceedings of the 8th Conference on Applied Climatology, California, pp. 179–184.
Marengo, J.A., Chou, S.C., Kay, G., Alves, L.M., Pesquero, J.F., Soares, W.R., Santos, D.C., Lyra, A., Sueiro, G., Betts, R., Chagas, D.J., Gomes, J.L., Bustamante, J.F., Tavares, P., 2011. Development of regional future climate change scenarios in South America using the Eta CPTEC/HadCM3 climate change projections: climatology and regional analyses for the Amazon, São Francisco and the Parana River Basins. Clim. Dyn. 38, 1829–1848.
Marengo, J.A., Liebmann, B., Grimm, A.M., Misra, V., Silva Dias, P.L., Cavalcanti, I.F.A., Carvalho, L.M.V., Berbery, E.H., Ambrizzi, T., Vera, C.S., Saulo, A.C., Nogués-Paegle, J., Zipser, E., Seth, A., Alves, L.M., 2012. Recent developments on the South American monsoon system. Int. J. Climatol. 32, 1–20.
Marsland, S.J., Haak, H., J Jungclaus, J.H., Latif, M., Röske, F., 2003. The Max- Planck-Institute global ocean/sea ice model with orthogonal curvilinear coordinates. Ocean Modell. 5, 91–127.
Mendes, M.C.D., Trigo, R.M., Cavalcanti, I.F.A., DaCamara, C.C., 2008. Blocking Episodes in the Southern Hemisphere: Impact on the Climate of Adjacent Continental Areas, Pure Appl. Geophys. 165, 1941–1962.
Menéndez, C.G., Carril, A.F., 2010. Potential changes in extremes and links with the Southern Annular Mode as simulated by a multi-model ensemble. Climatic Change 98, 359–377.
Menéndez, C.G., de Castro, M., Boulanger, J.P., D'Onofrio, A., Sanchez, E., Sörensson, A.A., Blazquez, J., Elizalde, A., Jacob, D., Le Treut, H., Li, L.Z.X., Nuñez, M.N., Pessacg, N., Pfeiffer, S., Rojas, M., Rolla, A., Samuelsson, P., Solman, S.A., Teichmann, C., 2010a. Downscaling extreme month-long anomalies in southern South America. Clim. Change 98, 379–403.
Menéndez, C.G., de Castro, M., Sörensson, A.A., Boulanger, J.P., 2010b. participating CLARIS Modeling Groups CLARIS Project: towards climate downscaling in South America. Meteorol. Z. 19, 357–362.
Nakicenovic, N. et al., 2000. IPCC Special Report on Emissions Scenarios. Cambridge University Press, p. 599.
Nogués-Paegle, J., Mo, K.C., 1997. Alternating wet and dry conditions over South America during summer. Mon. Wea. Rev. 125, 279–291.
Nogués-Paegle, J., Byerle, L.A., Mo, K.C., 2000. Intraseasonal modulation of South American summer precipitation. Mon. Wea. Rev. 128, 837–850.
Pascale, J., Damario, E., 1977. El Balance Hidrológico Seriado y su utilización en estudios agroclimáticos. Rev. Fac. Agron. La Plata (3a época) 53 (1–2), 15–34.
Pántano, V., Spescha, L., Penalba, O., Murphy, G., in press. Influencia de la variabilidad de la temperatura y la precipitacion en el agua del suelo, en la región oriental de secano de Argentina. Meteorologica (2014).
Penalba, O.C., Vargas, W.M., 2004. Interdecadal and interannual variations of annual and extreme precipitation over central-northeastern Argentina. Int. J. Climatol. 24, 1565–1580.
Penalba, O., Rivera, J.A., 2013. Future Changes in Drought Characteristics over Southern South America Projected by a CMIP5 Multi-Model Ensemble. American Journal of Climate Change 2, 173–182.
Penalba, O.C., Rivera, J.A., Pantano, V.C., 2014. The CLARIS LPB database: constructing a long-term daily hydro-meteorological dataset for La Plata Basin, Southern South America. Geoscience Data Journal 1, 20–29.
Pisciottano, G., Díaz, A., Cazess, G., Mechoso, C.R., 1994. El Niño Southern Oscillation Impact on Rainfall in Uruguay. J. Clim. 7, 1286–1302.
Rayner, N.A., Parker, D.E., Horton, E.B., Folland, C.K., Alexander, L.V., Rowell, D.P., Kent, E.C., Kaplan, A., 2003. Global analyses of sea surface temperature, sea ice, and night marine air temperature since the late nineteenth century. J. Geophys. Res. 108 (D14), 4407.
Re, M., Barros, V.R., 2009. Extreme rainfalls in SE South America. Climatic Change 96, 119–136.
Rivera, J.A., Penalba, O.C., 2011. Comparison of the performance of five indices for drought characterization in La Plata Basin. Perspectives towards a multi-scale monitoring system. In: WCRP Open Science Conference, Denver, USA, 23–27 October 2011.
Robertson, A.W., Mechoso, C.R., 1998. Interannual and decadal cycles in river flows of southeastern South America. J. Clim. 11, 2570–2581.
Robertson, A.W., Mechoso, C.R., 2000. Interannual and interdecadal variability of the South Atlantic convergence zone. Mon. Wea. Rev. 128, 2947–2957.
Robledo, F., Penalba, O., Bettolli, M.L., 2013. Teleconnections between tropical-extratropical oceans and the daily intensity of extreme rainfall over Argentina. Int. J. Climatol. 33, 735–745.
Rodrigues, D.A., Cavalcanti, I.F.A., 2006. Simulations of the Hydrologic Cycle over Southern South America using the CPTEC/COLA AGCM. Journal of Hydrome. 7, 916–936.
Roeckner, E., Arpe, K., Bengtsson, L., Christoph, M., Claussen, M., Dumenil, L., Esch, M., Giorgetta, M., Schlese, U., Schulzweida, U., 1996. The atmospheric general circulation model ECHAM4: model description and simulation of present-day climate: Max-Planck Institut für Meteorologie, Report no. 218, Hamburg, 86 pp.
Roeckner, E., Coauthors, A., 2003. The atmospheric general cir-culation model ECHAM5, Part I: Model description. Max-Planck-Institut Meteorol. Rep. 349, 127.
Ruscica, R.C., Sörensson, A.A., Menéndez, C.G., 2014. Hydrological links in Southeastern South America: soil moisture memory and coupling within a hot spot. Int. J. Climatol., 101002/joc.3930.
Saji, N.H., Yamagata, T., 2003. Possible impacts of Indian Ocean dipole mode events on global climate. Clim. Res. 25 (2), 151–169.
Saji, N.H., Ambrizzi, T., Ferraz, S.E.T., 2005. Indian Ocean dipole mode events and austral surface temperature anomalies. Dyn. Atmos. Oceans 39, 87–102.
Salio, P., Nicolini, M., Zipser, E.J., 2007. Mesoscale convective systems over Southeastern South America and their relationship with the South American low level jet. Mon. Wea. Rev. 135, 1290–1309.
Samuelsson, P., Jones, C., Willén, U., Ullerstig, A., Gollvik, S., Hansson, U., Jansson, C., Kjellstron, E., Nikulin, G., Wyser, K., 2011. The Rossby Centre Regional Climate Model RCA3: model description and performance. Tellus 63A, 4–23.
Sánchez, E., Gallardo, C., Gaertner, M.A., Arribas, A., Castro, M., 2004. Future climate extreme events in the Mediterranean simulated by a regional climate model: a first approach. Global Planet. Change 44, 163–180.
Sánchez, E., Domínguez, M., Romera, R., de la Franca, N.L., Gaertner, M.A., Gallardo, C., Castro, M., 2011. Regional modeling of dry spells over the Iberian Peninsula for present climate and climate change conditions. Climatic Change 107, 625–634.
Shahid, S., Behrawan, H., 2008. Drought risk assessment in the western part of Bangladesh. Nat. Hazards 46, 391–413.
Silvestre, G.E., Vera, C.S., 2003. Antarctic oscillation signal on precipitation anomalies over southeastern South America. Geophys. Res. Lett. 30, 2115–2118.
Silva, V.B.S., Berbery, E.H., 2006. Intense rainfall events affecting the La Plata basin. J. Hydrometeor 7, 769–787.
Smith, T.M., Reynolds, R.W., Peterson, T.C., Lawrimore, J., 2008. Improvements to NOAA's historical merged land-ocean surface temperature analysis (1880–2006). J. Clim. 21, 2283–2296.
Solman, S., Pessacg, N., 2012. Regional climate simulations over South America: sensitivity to model physics and to the treatment of lateral boundary conditions using the MM5 model. Clim. Dyn. 38, 281–300.
Solman, S., Sanchez, E., Samuelsson, P., da Rocha, R.P., Li, L., Marengo, J.A., Pessacg, N.L., Remedio, A.R.C., Chou, S.C., 2013. Evaluation of an ensemble of regional climate model simulations over South America driven by the ERA-Interim reanalysis: model perfor-mance and uncertainties. Clim. Dyn. 41, 1139–1157.
Sörensson, A.A., Menéndez, C.G., 2011. Summer soil-precipitation coupling in South America. Tellus Ser. A: Dyn. Meteorol. Oceanogr. 63, 56–68.
Taschetto, A.S., Ambrizzi, T., 2012. Can Indian Ocean SST anomalies influence South American rainfall? Clim. Dynam. 38, 1615–1628.
Tedeschi, R.G., Cavalcanti, I.F.A., Grimm, A.M., 2013. Influences of two types of ENSO on South American precipitation. Int. J. Climatol. 33, 1382–1400.

Tedeschi, R.G., Grimm, A.M., Cavalcanti, I.F.A., 2014. Influence of Central and East ENSO on extreme events of precipitation in South America during austral spring and summer. Int. J. Climatol., 101002/joc.4106.

Thornthwaite, C.W., Mather, J.R., 1957. Instructions and tables for computing potential evapotranspiration and water balance. Drexel Institute of Technology. Publications in Climatology, vol. X, pp. 185–311.

Thom, H.C.S., 1958. A note on the Gamma distribution. Mon. Wea. Rev. 86, 117–122.

Trenberth, K.E., 2011. Changes in precipitation with climate change. Clim. Res. 47, 123–138.

Uppala, S.M. et al., 2005. The ERA-40 re-analysis. Quart. J. R. Meteorol. Soc. 131, 2961–3012.

Vasconcellos, F.C., Cavalcanti, I.F.A., 2010. Extreme precipitation over Southeastern Brazil in the austral summer and relations with the Southern Hemisphere annular mode. Atmos. Sci. Lett. 11, 21–26.

Velasco, I.Y., Fritsch, J.M., 1987. Mesoscale convective complexes in the Americas. J. Geophys. Res. 92, 9591–9613.

Vera, C.S., Vigliarolo, P.K., Berbery, E.H., 2002. Cold season synoptic-scale waves over subtropical South America. Mon. Wea. Rev. 130, 684–699.

Vera, C.S., Higgins, W., Amador, J., Ambrizzi, T., Garreaud, R., Gochis, D., Gutzler, D., Lettenmaier, D., Marengo, J.A., Mechoso, C.R., Nogués-Paegle, J., Silva Dias, P.L., Zhang, C., 2006. Toward a unified view of the American Monsoon systems. J. Clim. 19, 4977–5000.

Wang, C., 2002. ENSO and atmospheric circulation cells. CLIVAR Exchanges 7, 9–11.

Yeh, S.W., Kug, J.S., Dewit, B., Kwon, M.H., Kirtman, B., Jin, F.F., 2009. El Niño in a changing climate. Nature 461, 511–515.

Zamboni, L., Kucharski, F., Mechoso, C.R., 2012. Seasonal variations of the links between the interannual variability of South America and the South Pacific. Clim. Dynam. 38, 2115–2129.

Zamboni, L., Mechoso, C.R., Kucharski, F., 2010. Relationships between upper-level circulation over South America and Rainfall over Southeastern South America. J. Clim. 23, 3300–3315.